

2001

Contact electrification of copolymers and surface charge stability models

Ken Q. Vo
San Jose State University

Follow this and additional works at: https://scholarworks.sjsu.edu/etd_theses

Recommended Citation

Vo, Ken Q., "Contact electrification of copolymers and surface charge stability models" (2001). *Master's Theses*. 2161.
DOI: <https://doi.org/10.31979/etd.h7bn-2jfr>
https://scholarworks.sjsu.edu/etd_theses/2161

This Thesis is brought to you for free and open access by the Master's Theses and Graduate Research at SJSU ScholarWorks. It has been accepted for inclusion in Master's Theses by an authorized administrator of SJSU ScholarWorks. For more information, please contact scholarworks@sjsu.edu.

INFORMATION TO USERS

This manuscript has been reproduced from the microfilm master. UMI films the text directly from the original or copy submitted. Thus, some thesis and dissertation copies are in typewriter face, while others may be from any type of computer printer.

The quality of this reproduction is dependent upon the quality of the copy submitted. Broken or indistinct print, colored or poor quality illustrations and photographs, print bleedthrough, substandard margins, and improper alignment can adversely affect reproduction.

In the unlikely event that the author did not send UMI a complete manuscript and there are missing pages, these will be noted. Also, if unauthorized copyright material had to be removed, a note will indicate the deletion.

Oversize materials (e.g., maps, drawings, charts) are reproduced by sectioning the original, beginning at the upper left-hand corner and continuing from left to right in equal sections with small overlaps.

Photographs included in the original manuscript have been reproduced xerographically in this copy. Higher quality 6" x 9" black and white photographic prints are available for any photographs or illustrations appearing in this copy for an additional charge. Contact UMI directly to order.

ProQuest Information and Learning
300 North Zeeb Road, Ann Arbor, MI 48106-1346 USA
800-521-0600

UMI[®]

**CONTACT ELECTRIFICATION OF COPOLYMERS AND SURFACE CHARGE
STABILITY MODELS**

A Thesis

Presented to

**The Faculty of the Department of Chemical/Materials Engineering
San Jose State University**

In Partial Fulfillment

of the Requirements for the Degree

Master of Science

By

Ken Q. Vo

May 2001

UMI Number: 1403994

Copyright 2001 by
Vo, Ken Quan

All rights reserved.

UMI[®]

UMI Microform 1403994

Copyright 2001 by Bell & Howell Information and Learning Company.

All rights reserved. This microform edition is protected against
unauthorized copying under Title 17, United States Code.

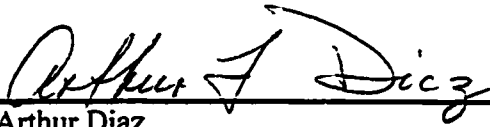
Bell & Howell Information and Learning Company
300 North Zeeb Road
P.O. Box 1346
Ann Arbor, MI 48106-1346

© 2001

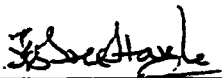
Ken Q. Vo

ALL RIGHTS RESERVED

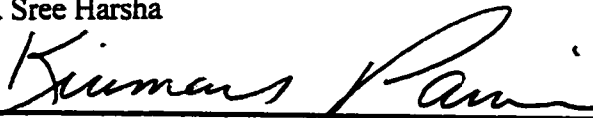
APPROVED FOR THE DEPARTMENT OF
CHEMICAL/MATETERIALS ENGINEERING



Dr. Arthur Diaz

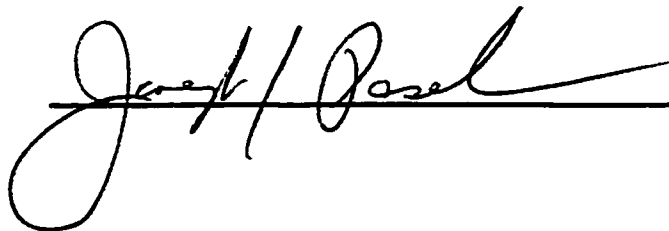


Dr. Sree Harsha



Dr. Kiumars Parvin

APPROVED FOR THE UNIVERSITY



**Part of this thesis was selected to represent SJSU in the
14th Annual system-wide
2000 CSU Student Research Competition
at
California Polytechnic University, Pomona**

ABSTRACT

A contact electrification (C.E.) experiment was performed to confirm the presence of mobile charge on three copolymers, sulfonated polystyrene-butylmethacrylate copolymer (SS-BUMA), sodium salt of sulfonated polystyrene-butylmethacrylate copolymer (SS-BUMA Na Salt), and polystyrene-2-vinylpyridine copolymer (PS-2-VP). The contact materials were either metal or vinyl and the contacts were in the form of gentle touch, swipe and rub. The surface potential was measured before and after contact to indirectly monitor any evidence of charge transfer. The Monroe Electronics Isoprobe (non-contact) Electrostatic Voltmeter 244 was used to measure the surface potential. The surface potential measurements confirmed the presence of the mobile charge with SS-BUMA and Na Salt SS-BUMA and the sign of the mobile charges were positive with both polymers. The reverse in polarity due to contact electrification was not observed for PS-2-VP and charge transfer could not be confirmed.

ACKNOWLEDGEMENT

I would like to express my utmost and profound gratitude to my research advisor Dr. A. Diaz. This thesis is not possible without his decisive and clear guidance from beginning to end. With his competitive and courageous influence we have received nomination to use part of this thesis to take part in a research competition at the state level. In addition I want to sincerely thank Dr. K. Sreeharsha and Dr. K. Parvin for their unconditional supports of this thesis. It is their involvement that has made this thesis possible.

TABLE OF CONTENTS

LIST OF SYMBOLS.....	ix
LIST OF TABLES.....	x
LIST OF FIGURES.....	xi
Chapter 1 - Introduction.....	1
Chapter 2 - Background	
2.1 Surface charge stability.....	3
2.2 Contact electrification.....	5
2.3 Physical quantities associated with surface charge.....	9
Chapter 3 - Literature Review	
3.1 Case studies of surface charge decay through the material (leak through)....	13
3.2 Case studies of surface charge decay through air (discharge).....	21
3.3 Case studies of surface charge decay across the surface (run-off).....	25
Chapter 4 – Electrification Apparatus	
4.1 System make-up.....	31
4.2 Materials used to test electrification apparatus.....	33
4.3 Test Procedures.....	35
Chapter 5 – Data Analysis	
5.1 Analysis for stage 1 – Validating instrument functionality and repeatability.....	36
5.2 Analysis for stage 1 – Oscillatory signal Pattern.....	41
5.3 Analysis for Stage 2 – Confirming C.E. from potential’s polarity.....	45

TABLE OF CONTENTS

5.4 Analysis for stage 2 – Measuring maximum surface potential under C.E.....	47
5.5 Analysis for Stage 2 – Pressure effect.....	48
Conclusion.....	53
Appendix I – Derivation of Equation 2.....	54
Appendix II – Electrification Apparatus Operating Manual.....	57
References.....	60

LIST OF SYMBOLS

Symbols

α	Injection coefficient
C	Capacitance
E	Electricfield
ε	Permittivity
ε_0	Permittivity of space
ϕ	Potential
Q	Electric charge
ρ	Resistivity
σ	Surface charge density
V	Potential

LIST OF TABLES

Table 1. Relevant informational summary of articles.....	14
Table 2. Summary of electrical properties related to surface charge conduction.....	26
Table 3. Summary of material structure, their charge characteristics relevant to C.E.....	34
Table 4. Surface potential polarity as a result of pellet formation.....	46
Table 5. Surface potential prior to and after C.E. with the associated contacting material.....	48

LIST OF FIGURES

Figure		Page
1.	Charge dissipation paths	4
2.	Kinds of contacts as discussed by Harper	6
3.	Contact charging taking place between two objects. Objects are oppositely charged after separation	7
4.	Order of magnitude of contact charging of different materials as a function of pressure between surface.....	8
5.	Electric field due to an elemental surface area da' with a surface charge density $\sigma(r')$ on the surface S'	9
6.	Non uniform of charge density on surface of an insulator	12
7.	Capacitor configuration for modeling of surface charge decay.....	16
8.	Regions of the electric field in the sample.....	18
9.	Experimental data of Ieda et al. Showing an initial field dependence of the decay curves and crossing.....	18
10.	Experimental data by Coelho confirmed charge injection effect on decay. (\square) charge injection only, (\blacklozenge) charge injection with latent surface charges.....	20
11.	Electric field in the air gap.....	22
12.	Charge decay through ionized air from a surface.....	23
13.	Simplified drawing of Faraday cage of cross section.....	27
14.	Measured voltage signals revealing a surface charge decay.....	29
15.	$1/V$ versus time plots for various materials.....	30
16.	Basics components of electrification apparatus.....	31
17.	Voltage readings of air and grounded metal surface.....	37

LIST OF FIGURES – continues

Figure	Page
18. Repeatability of surface potential measurements of PS-2-VP.....	38
19. Repeatability of surface potential measurements of SS-BUMA Na Salt.....	39
20. Repeatability of surface potential measurements of SS-BUMA.....	40
21. Surface potential of PS-2-VP pallet-form sample as a function of time.....	42
22. Surface potential of SS-BUMA-Na Salt pallet-form sample as a function of time.....	43
23. Surface potential of SS-BUMA pallet-form sample as a function of time.....	44
24. Evolution of the contact electrification data in terms of surface potential versus number of contact for SS-BUMA.....	49
25. Schematic of pallet making device and process.....	50
26. Evolution of the contact electrification data in terms of surface potential versus number of contact for SS-BUMA Na Salt.....	51
27. Evolution of the contact electrification data in terms of surface potential versus number of contact for PS-2-VP.....	52
28. Calculation of the field due to a uniform infinite plane sheet.....	54
29. Schematic of electrification apparatus.....	57
30. Direction switch layout for SK1 Stepper Driver.....	57
31. Pin connection configuration for controlling SK1 Stepper Driver.....	58
32. Connection from Isoprobe Eletrostatic Voltmeter to DAQ Pad 1200.....	59

CHAPTER 1 – INTRODUCTION

1.1 Thesis objectives

This chapter reports the objectives of this thesis. It highlights the issues and significance of surface charges in applications for the home, offices, up to high-tech laboratory.

This thesis addresses two aspects of surface charge on polymers: stability of surface charge, and generation of charge by contact electrification (C.E.). The study on the stability of surface charge involves the discussion of some of the relevant models for charge decay. The key parameters affecting the decay process are identified. The study of C.E. is limited to the charge on the surface of a polymer generated by a metal-polymer contact. This study involves the use of an electrification apparatus to determine the maximum amount of surface charge that can be generated on selected polymers via multiple contacts. The experimental maximum amount of surface charge deposited is compared with the derived theoretical value. Materials considered here are SS-BUMA, SS-BUMA Na salt, and PS-2-VP.

Both surface charge stability and C.E. are important in many commercial applications. For example, in the area of xerography where toner particles are charged by contact (C.E.), the efficiency of the charging process and surface charge stability are important. In semiconductor processing, polymer films formed on machine parts and device parts are highly susceptible to developing surface charge. This is often a serious problem. One of the effects of surface charges is the deterioration of the etching profile of contact and via of semiconductor devices caused by the electric fields generated from

the surface charge. These fields can alter the path of the species to cause non-straight etch profile (e.g. notches, and trenches). Other related applications are found in areas of precipitation (e.g. electrofilter, and ionizers), and electrical insulation just to mention a few.

CHAPTER 2 – BACKGROUND

2.1 Surface charge stability

In this chapter the three modes of charge decay are discussed. In section 2.2 the definition of contact electrification is presented and discussed base on the views provided by Harper (6). Additionally, various environmental effects on the quantity of charge transferred are presented. Section 2.3 reports the formulations of physical quantities that are associated with surface charge are presented, i.e. surface potential, electric field.

Surface charge stability is determined by the conditions and mechanisms for dissipation of surface charges. Charge dissipation or the removal the built-up charge, is very dependent on the material compositions, electrical properties and electric fields inside and outside the materials. In general, surface charges dissipate via three paths. Charges can leak through the material itself (leak-through), along the surface (run-off), or across an air gap (discharge). These paths are diagrammed in Figure 1. Leak-through could result from drift (under influence of an electric field), diffusion, tunneling, or under low level conductivity. Charge decay through the air gap, also referred to as discharge, is very dependent on the electric field E created by the charges on the surface. If E exceeds the breakdown electric field of air, E_b ($E_b = 3.0 \times 10^6 \text{ V m}^{-1}$), the air between the charged surface and a grounded electrode is ionized to produce ions which move to the surface to neutralize some of the surface charge. The field necessary and initiate the discharging through the air is dependent on the surface charge density, $q / A = \sigma$, and the atmosphere (e.g. humidity).

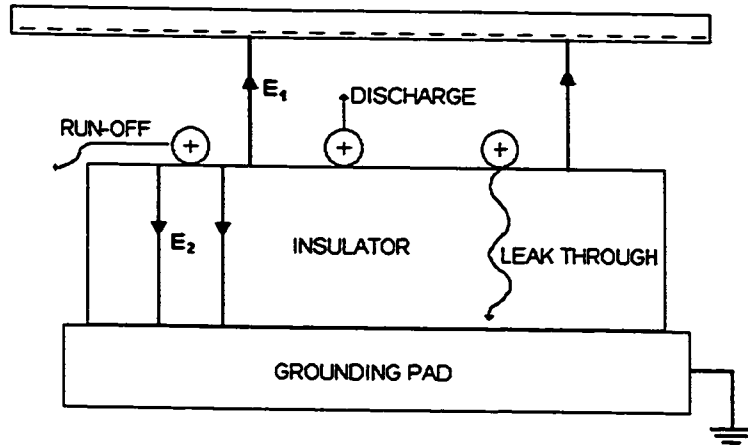


Figure 1. Charge dissipation paths.

2.2 Contact electrification

C.E. refers to the process of depositing charges (positive or negative) on the surface of conducting as well as non-conducting materials by a “gentle” contact. These charges can be due to electrons or ions. The electron is charged negative and the ion can be either positive or negative. In C.E., the charges produced on the surface are often near localized and immobilized at the site of contact. Charge deposition on surfaces can also be achieved by exposing a surface to a corona discharge, under an electron beam, or by contacting two different surfaces. In this thesis, only contact charging will be addressed.

In C.E., the contact can occur by touching, sliding, rubbing, with or without friction, with or without pressure (loading), or by any combination of these. As a matter of fact, there is great complexity in the words used to describe contact. A discussion by Harper (6) on the different types of contact is diagrammed in Figure 2. In this diagram, we added the distance axis to show that the various types of contact are organized by the closest proximity between the two surfaces at contact.

Apparent contact refers to a casual observation of contact, but in fact there may be no contact. Only under more careful inspections can some form of a contact be verified. Real contact refers to contact with mechanical actions and reactions between the surfaces. If mechanical forces are transferred from one surface to the other through an intermediate body between the surfaces, then the contact is referred to as impeded contact. Without the presence of the intermediate body, the contact is referred to as intimate contact, and it can either be close contact or true contact. In close contact, mechanical forces are

transmitted between the surfaces by long-range molecular forces. In true contact, the mechanical forces are transmitted by short-range molecular forces. Finally, true contact can be categorized as molecular contact or direct contact. Molecular contact is a type of true contact in which short-range repulsive forces exist, and these short-range repulsive forces exist when a film with composition different from the substrate is present on the surface. However, if no surface films are present, i.e. no short-range repulsive forces, the true contact will be a direct contact. The different contact classifications are related to the separation distances between the two bodies. However, different physical forces are also involved at each level of contact, e.g. electrostatic, and van der Waals.

In the C.E. processes, shown schematically in Figure 3, charge particles (electrons and/or ions) are transferred between the surfaces of the two objects. Under specific conditions charged pieces of the material itself may be transferred. After the objects separate, the charge particles remaining on the surface of each object will have a net charge with opposite polarity.

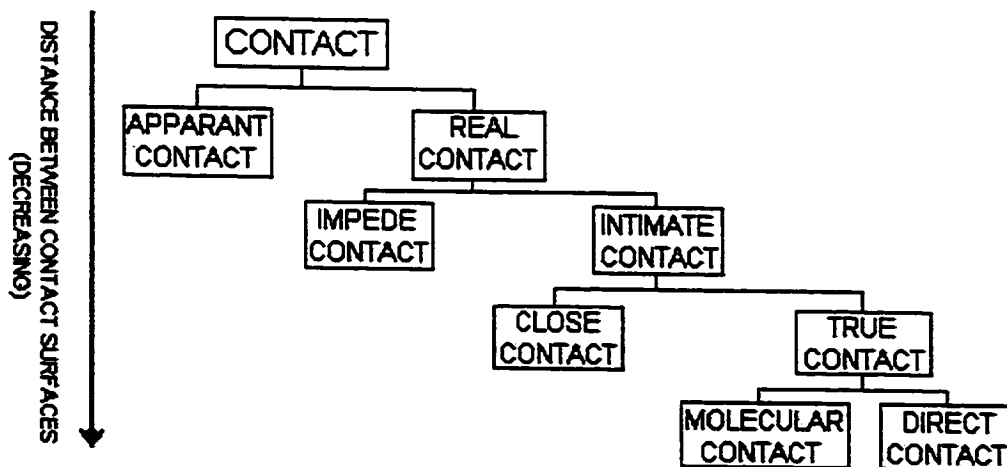


Figure 2. Types of contacts as discussed by Harper [6].

Many factors influence the amount of charge that deposits on surfaces in contact charging. Smooth surfaces tend to produce more contact charge than rough surfaces. Roughness and pressure also affect the amount of surface charge as shown in Figure 4. The pressure effect can be explained by influence of pressure on the energy barrier that prevents charge transfer. The roughness effect is predicted to be associated with the materials transfer mechanism. I anticipate that more roughness will result in more material transfer during C.E.. Frictions, which are associated with the contacts, influence the amount of charge because friction can alter the conditions of the contact area. The dielectric constant of the material also affects the outcome of the contact process, where materials with a higher dielectric constant tend to charge positively. The total charge deposited is also affected by the environmental conditions (e.g. humidity, presence of ions), materials compositions, material structures (e.g. crystalline structures, polymer chain length, polymer side groups), surface and bulk impurities, and work function of the metal contact used.

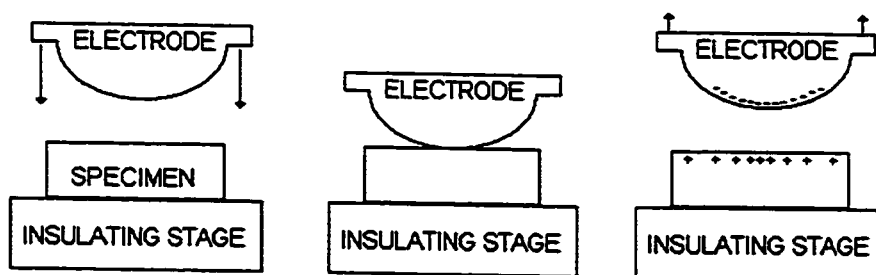


Figure 3. Contact charging taking place between two objects. Objects are oppositely charged after separation.

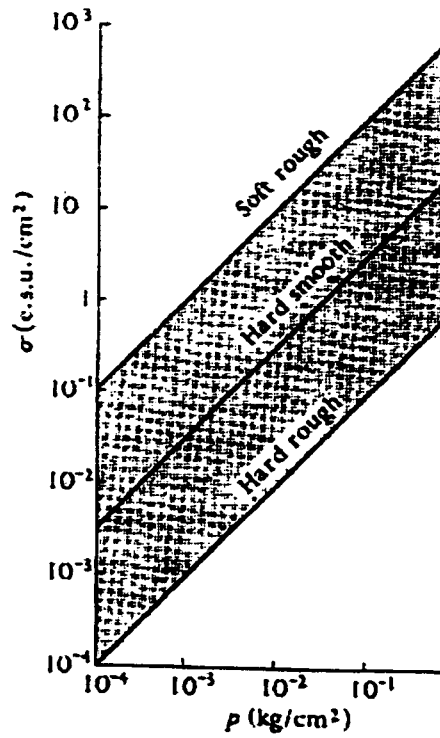


Figure 4. Order of magnitude of contact charging of different materials as a function of pressure between surfaces. From Harper [6]. Reprinted with permission from Oxford University Press.

2.3 Physical quantities associated with surface charge

Per discussion by Wangness (10), the presence of a charge on the surface of either a conductor or an insulator produces an electric field that is pointing away from the surface. The electric field, E , at a point near the surface is proportional the surface charge density, σ , and R , the distance between the charge source and the location where E is measured as shown in Figure 5. The electric field is defined by Equation 1. Note that the surface charge density, $\sigma(r')$, is a function of position on the surface, i.e. $\sigma(r')$ is not uniform in general. r' is the distance from a referenced origin to the charge source as shown in Figure 5. For teaching and real world analysis, Equation 1 is often carried out in simplified form. A first step in is to assume that the surface charge density is constant, i.e. $\sigma(r') = \sigma = \text{constant}$. The second step is to choose a surface geometry with symmetry and non-practical (i.e. infinite in dimensions). For example, the electric field in V/m at a point perpendicular to the surface of an infinite plane with a constant surface charge is given Equation 2. The derivation of Equation 2 is given in Appendix I.

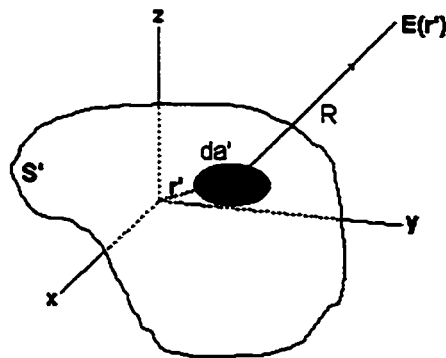


Figure 5. Electric field due to an elemental surface area da' with a surface charge density $\sigma(r')$ on the surface S' which is not necessary flat.

$$E(r) = \frac{1}{4\pi\epsilon_0} \int_{S'} \frac{\sigma(r')\hat{R}da'}{R^2} \quad (1)$$

ϵ_0 = permittivity of space = 8.854×10^{-12} F/m

$\sigma(r')$ = surface charge density at r'

S' = surface

\hat{R} = radial unit vector

$$E_{\text{infinite plane}}(z) = \frac{\sigma}{2\epsilon_0} \quad (2)$$

Another example of an application of Equation 1 is the calculation of the electric field at any point between two infinite plane sheets with constant opposite surface charge density. For this configuration, the electric field, which is perpendicular to the sheet plane, anywhere between the two sheets is given by Equation 3. Equation 2 and 3 can be safely applied to real-world cases under specific conditions.

$$E_{\text{Two infinite planes}}(z) = \frac{\sigma}{\epsilon_0} \text{ [V/m]}. \quad (3)$$

Another physical quantity associated with the surface charge is the electrical potential, or the potential, which measures the amount of energy per unit charge to move one charge q ($q = 1.602 \times 10^{-19}$ C). The electric potential is defined by Equation 4. In terms of the surface charge density, the general expression for the surface potential is given by Equation 5. The relationship between the electric field E and the surface potential ϕ is given by Equation 6.

$$\text{Electric potential} = \phi = \frac{\text{Energy}}{q}. \quad (4)$$

$$\phi(r) = \frac{1}{4\pi\epsilon_0} \int_s \frac{\sigma(r') da'}{R}. \quad (5)$$

$$E = -\nabla\phi. \quad (6)$$

Again, it is convenient to assume constant surface charge density σ and symmetrical configuration of the system, e.g. spherical surface or infinite plane sheet. As an example, the potential difference between two infinite plane sheets with opposite surface charge density is given by Equation 7. A variation of Equation 7 is given by Equation 8. In these equations, d is the distance between the two plates in the capacitor system.

$$\phi_2 - \phi_1 = V = Ed = \frac{\sigma}{\epsilon_0} d \quad (7)$$

$$V = Ed = \frac{\sigma}{\epsilon_0} d \quad (8)$$

The electrostatic energy associated with the surface charge is given by Equation 8. Applying Equation 8 to the case of two infinitely plane sheets with opposite constant surface charge density, the electrostatic energy density for this system is given by Equation 9. Equations 3, 7 and 9 are important when describing discharge. For example, when the electric field as given by Equation 3 exceeds the break down field of the surrounding air, discharge will occur.

$$U = \frac{1}{2} \int_S \sigma(r) \phi(r) da \quad (8)$$

$$\frac{U}{\text{Volume}} = \frac{1}{2} \epsilon_0 E^2 = \frac{\sigma^2}{2\epsilon_0} \quad (9)$$

Note that Equations 3, 7 and 9 assume constant surface charge, which is not generally true, because the surface charge density on insulating materials is not evenly distributed. For example the surface potential at the point P_1 may be different from point P_2 in Figure 6. The potential at P_1 might be +200V while that at P_2 might be -40V. The surface potential, electric field as well as the energy will depend upon both the charge at the point in question plus the distribution of charges over the remainder of the insulator. Thus, in order to apply Equations such as 3, 7 and 9 for the case of an insulator, attention must be given to closely match the conditions for deriving at the equations and the conditions of the materials under investigation.

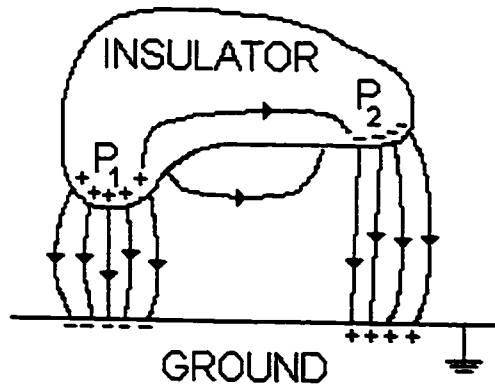


Figure 6. Non uniform of charge density on surface of an insulator.

CHAPTER 3 – LITERATURE RESEARCH

3.1 Case study of surface charge decay through the bulk (leak-through)

This section reports the summary of theoretical models as well as experimental results of surface charge decay. Section 3.1 contains discussion of the leak-through charge decay mode. Section 3.1 contains discussion of the discharge decay mode. Section 3.1 contains discussion of the run-off decay mode.

Relevant discussions of surface charge decay through the bulk material were found among four articles. Key information from these reports is summarized in Table 1, which lists the materials, sample thickness, sample configuration, charging mode, and decay path considered by each study. In all four studies no external field was applied to the sample so that charges decay to the grounded electrode was driven by the electric field generated by the “deposit” charges themselves. “Deposit” charges are charges that are intentionally put on the sample surface via contact charging, corona charging, or from and ion beam. For all four studies the initial electric field produced by the deposited charges ranged from 200V – 10kV.

Models for surface charge decay as reported by Ieda (7) and Coelho (2) were based on a capacitor model. In this model an electric field is present as a result of the deposited surface charge and counter charge on the grounded electrode. The capacitor configuration is shown in Figure 6. Ieda (7) proposed an exponential decay of the surface charge, in which he assumed constant resistivity, ρ , and time independent capacitance, C . The decay is expressed in terms of the surface potential given by Equation 10, where V_0

is related to an initial field E_0 and is given by $E_0 = V/d$. A schematic for this model is shown in Figure 7. ϵ_0 and ϵ are the permittivity of air and of the material respectively, and d is the thickness of the sample. Differently, Coelho (2) used the Poole-Frenkel voltage dependent resistivity, which is given by Equation 11, with $\epsilon_0 = 1$, and time independent capacitance, to report a surface potential decay as given by Equation 12.

Table 1. Relevant informational summary of articles

Article by...	Ieda et al.	Wintle	Coelho et al.	Coelho et al.
Materials	LDPE/active-agent doped PE	Polyethylene (PE)	Teflon FEP	Kapton Polyimide
Thickness	0.015 – 0.113mm		0.125 mm	0.050 mm
Configuration	Sample on grounded electrode	Sample on grounded electrode	Sample on grounded electrode	Sample on grounded electrode
Charging mode	Corona	Corona	Corona /electron beam	Electron beam
Decay path	Through sample	Through sample	Through sample	Through sample

In another discussion, Coelho (3) reported two models for surface potential decay based on space-charge considerations. Mainly, space-charge considerations involve the generation of the needed electric field by volume charge that drives the conduction of charge through the material. The Mobility Control Decay model (MCD), which assumes that all deposit charges are unobstructively injected into the materials and the MCD surface potential decay is given by Equation 13. The other model is called the Barrier Control Decay model. The BCD model assumes that not all surface charges are freely

injected. The surface potential in the BCD model is given by Equation 13 with the time constant τ defined by Equation 14.

$$V = V_o e^{-t/\tau} \quad (10)$$

$$\rho(V) = \rho_o \exp\left(-\frac{1}{2kT} \sqrt{\frac{e}{\pi\epsilon L}} \sqrt{V}\right) \quad (11)$$

$$\frac{dV}{dt} = -\frac{V}{\tau} \quad (12)$$

$$V(t) = \frac{\mu Q^2}{2\epsilon^2} (1 - t/\tau) = V_o (1 - t/\tau), \quad \tau = 2\epsilon L / \mu Q \quad (13)$$

$$\tau = \frac{\mu}{\epsilon^2} \alpha (1 - \alpha/2) Q^2 \quad (14)$$

Definition of symbols:

$\rho(V)$ = volume charge density as function of voltage

ρ_o = initial volume charge density

k = Boltzman constant = 1.386×10^{-23} J/K

T = absolute temperature

e = electrical charge = 1.602×10^{-19} C

L = thickness of the sample

ϵ = permittivity of the sample

μ = mobility of the sample

α = injection coefficient

Q = total charge per unit area

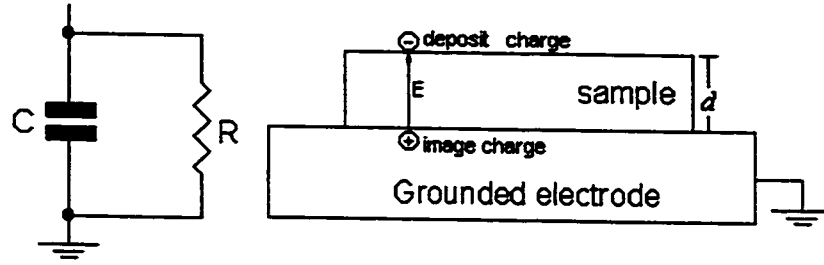


Figure 7. Capacitor configuration for modeling of surface charge decay.

Wintle's (12) model for surface charge decay is also based on space-charge.

Unlike Coelho (3), Wintle considered the mobility to be field-dependent and carrier-density-dependent, and the presence of deep trappings. The field-dependent mobility is given as $\mu = cE^{n-1}$, and surface potential is given by Equations 14a and 14b. The carrier-

density-dependent mobility is given as $\mu = h \frac{\partial E}{\partial x}$ and surface potential is given by

Equations 15a and 15b. When deep traps are present, the surface potential is given by

Equations 16a and 16b.

Equations for field-dependent mobility:

$$V_{\text{surface}}(t) = E_o \left[\frac{1}{2} \mu^2 \alpha + \frac{cE_o^n t n}{n+1} \right], \text{ for } (\alpha + cE_o^n t) < l \quad 14a$$

$$V_{\text{surface}}(t) = E_o \left[\frac{1}{2} \mu^2 \alpha + \frac{cE_o^n \mu^{n+1} t n}{n+1} \right], \text{ for } (\alpha + cE_o^n t) > l \quad 14b$$

Equations for carrier-density-dependent mobility:

$$V_{\text{surface}}(t) = E_o \left[\frac{1}{2} \mu^2 \alpha + \frac{cE_o^n t n}{n+1} \right], \text{ for } \left| \alpha + E_o (2ht)^{1/2} \right| < l \quad 15a$$

$$V_{\text{surface}}(t) = \frac{\frac{1}{2} E_o l^2}{\alpha + E_o (2ht)^{1/2}}, \text{ for } \alpha + E_o (2ht)^{1/2} > l \quad 15b$$

$$V_{\text{surface}}(t) = E_1 \left[l - \frac{1}{2} \left(\alpha + \left(p_o \alpha / p_{\text{trapped}} \right) (1 - e^{-t/\tau}) \right) \right], \text{ for } t < \tau \quad 16a$$

$$V_{\text{surface}}(t) = \frac{\frac{1}{2} q l^2 p_{\text{trapped charge}} / \epsilon \epsilon_o}{(1 - e^{-t/\tau})}, \text{ for } t > \tau \quad 16b$$

In these equations, α is the distant into the sample below the surface that can be reached by the deposited charges; l is the sample thickness, E_o is the field the region $l-\alpha$, E_1 is the field in the space-charge region, μ is the mobility, h is a constant of proportionality, $p_{\text{trapped charge}}$ is the trapped charge concentration and $\tau = \epsilon \epsilon_o / \mu q p_{\text{trapped charge}}$. For the above models, the charge distribution (i.e. electric field) configuration inside the materials prior to any charge decay process is shown schematically in Figure 8.

From the discussion of these models the following summary is attained. The electric field plays two roles in the charge decay process. First, the electric field is involved in the the initial charge decay as shown experimentally by Ieda. This influence of the initial field on the decay is shown in Figure 9. This effect was acknowledged by Coelho (2). Second, the electric can influence the resistivity and mobility, i.e. $\rho(E)$ or $\mu(E)$ of the material. The field-dependent mobility by $\mu = (\text{constant})E^{n-1}$ was reported by Wintle (11). The field-dependent resistivity was reported by Coelho (3) as seen in the

following equation: $\rho(V) = \rho_o \exp\left(-\frac{1}{2kT} \sqrt{\frac{e}{\pi \epsilon L}} \sqrt{V}\right)$.

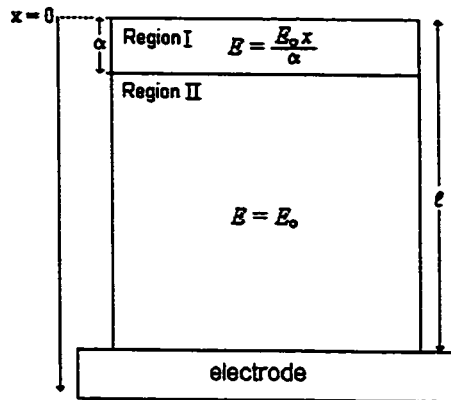


Figure 8. Regions of the electric field in the sample.

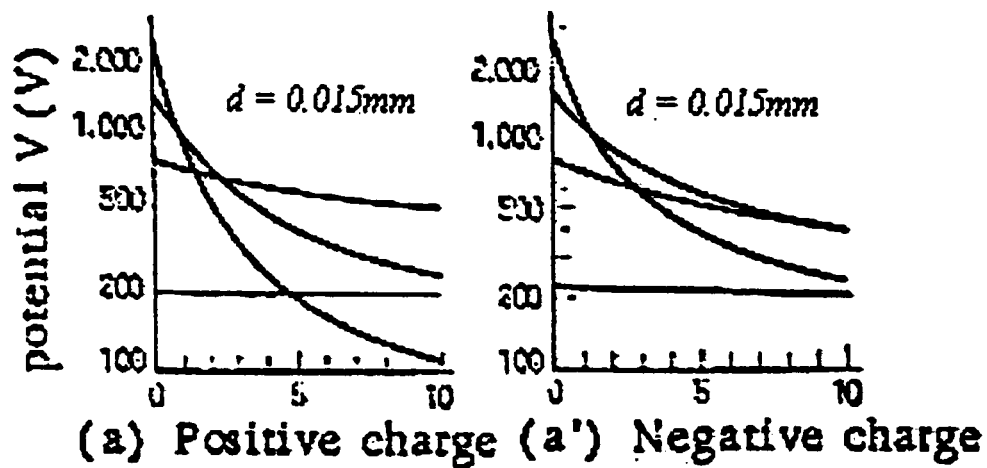


Figure 9. Experimental data showing an initial field dependence of the decay curves and crossing. From Ieda et al. [7]. Reprinted with permission from

As can be seen, the models for charge decay through the bulk take into account material properties such as ρ and μ . These parameters can be treated as constants (7) or they can be dependent on other physical aspects of the materials such as carrier density (12).

These studies did not specify the condition(s) when the models are valid or when the carrier-density dependency takes effect in the charge decay processes. Unfortunately,

information from the studies provided only a partial answer to the question of when and under what specific conditions the equations are applicable. That is, the field dependent of the mobility should be considered when there is a high electric field in the bulk.

Considerations in regards to the effect of charge injection on bulk-charge-decay were discussed by Coelho (3). The study confirmed that a faster decay rate occur when the charges are deposited “unobstructively”, and would have penetrated into interior of the bulk just below the surface. On the other hand, when the deposited charges encounter some form of an energy barrier as they penetrate below the material’s surface, the decay rate was relatively slower. This result is shown in Figure 10. From this discussion, I anticipate that the charge injection effect is dependent on the nature of charge deposition. When charges are deposited with high energy, via corona or an electron beam, charge injection could occur and the decay rate would be fast. However, when the deposited charges have low momentum, for example contact charging, charge injection would have little effect on the decay rate in the initial decay process.

Traps also affect the charge decay process. In regards to traps, Wintle (12) considered only the trapped charges. The initial carrier density is assumed to be large enough to fill all the traps in the bulk so that there are free carriers left to conduct through the bulk. The model does not address the release of trapped charges. Based on this study I concluded the following:

The initial charge decay rate will be affected by traps. When all traps are filled, the subsequent decay rate will then dependent on the material

properties. The charge release, will be dependent on temperature and appropriate release probability. The issue of trap should always be considered when dealing with charge decay in insulators because they are always present in insulator.

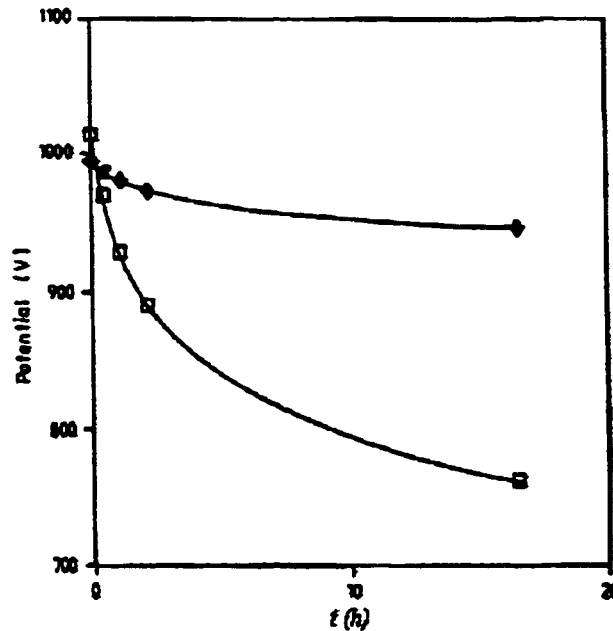


Figure 10. Experimental data by Coelho confirmed charge injection effect on decay. (□) charge injection only, (◆) charge injection with latent surface charges. From Coelho et al. [3]. Reprinted with permission from the Institute of Physics Publishing.

The authors point out that the transit time, the time for the first charges to reach the grounded electrode, is important because all activities such as charge trapping, and field-dependent mobility take place within the transit time. The transit time parameter was included in all studies except that of Ieda (7). The expression for the transit time differs from model to model. The transit time will always be proportional to the total deposit charge and the thickness and nature of the sample.

3.2 Case study of surface charge decay through air (discharge)

Two literature reports on discharge were found to be particularly relevant to this project. Coelho (2) considered surface charge decay through an air gap. Though no real applied field was considered, when the measuring probe, M , is turned on for measurement, the condition of applied field is met. The source of the electric field are the surface charges. The configuration of the sample with the associated plane charge and electric field is shown in Figure 11. The electric field, with the mobile surface plane charge in the air gap is given Equation 17. The measuring probe measured a current, resulting from migration of surface charge into the air. When the probe is just turned on, a constant current is immediately reached, which is given by Equation 18. Then the current decayed towards a saturation value given by Equation 19, assuming no collision in the gap.

$$E_{\text{air, with charge layer moving}} = \frac{\alpha x}{\epsilon_0 d + \epsilon D} \quad (17)$$

$$I_{\text{initial}} = Ne\mu ES \quad (18)$$

$$I_{\text{saturation}} = e d S \frac{dN}{dt} \quad (19)$$

In Equation 17-19, σ is the surface charge density, ϵ_0 is the permittivity of air, ϵ is the permittivity of the sample, d is the thickness of the sample, D is the air gap, N is the initial uniform concentration of ion pairs, μ is the average ionic mobility, S is area of the electrode, and dN/dt is the number of ions created per unit volume per second. The theoretical calculation of $I_{\text{initial, theoretical}}$ (2.2×10^{-11} A) and $I_{\text{saturation, theoretical}}$ (3.9×10^{-17} A) was calculated using $N = 10^3 \text{ cm}^{-3}$, $\mu = 1 \text{ cm}^2 \text{ V}^{-1} \text{ s}^{-1}$, $S = 28 \text{ cm}^2$, $E = 5 \times 10^3 \text{ V cm}^{-1}$. However, the experimental values ($I_{\text{initial, experimental}} \approx 10^{-12}$ A and $I_{\text{saturation, theoretical}} < 10^{-15}$ A) did not agree the theoretical values.

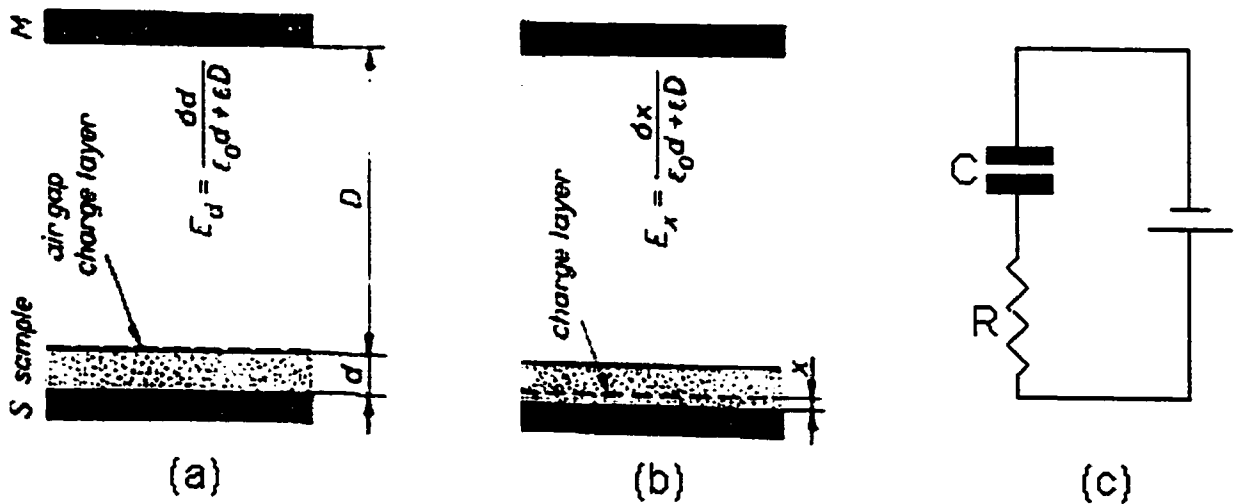


Figure 11. Electric field in the air gap. M is the measuring probe. S is the substrate. (a) System with charge plane at the surface of the sample. (b) Charge plane at a distance $x < d$ from the substrate. (c) Equivalent circuit. From Coelho et al. [2]. Reprinted with permission from IEEE.

The study of charge decay through the air reported by Jonassen involves no electrodes (8). The surface charges generate an electric field, which draws in ions from

the bulk which neutralize the surface charges. Furthermore, the electric field will force surface charges to leave the surface and conduct away through the ionized air. This is shown in Figure 12.

Jonassen's model considers an electric field generated by the surface charges, extending out from the surface as shown in Figure 12. The electric field, Equation 20, causes a current of positive ions, Equation 21, to flow away from the surface. Concurrently, a current density of negative ions, Equation 22, flows towards the surface. Equations 20-22 were then manipulated to attain an expression for positive-surface-charge decay as given by Equation 23. A similar expression exists for negative-surface-charge decay.

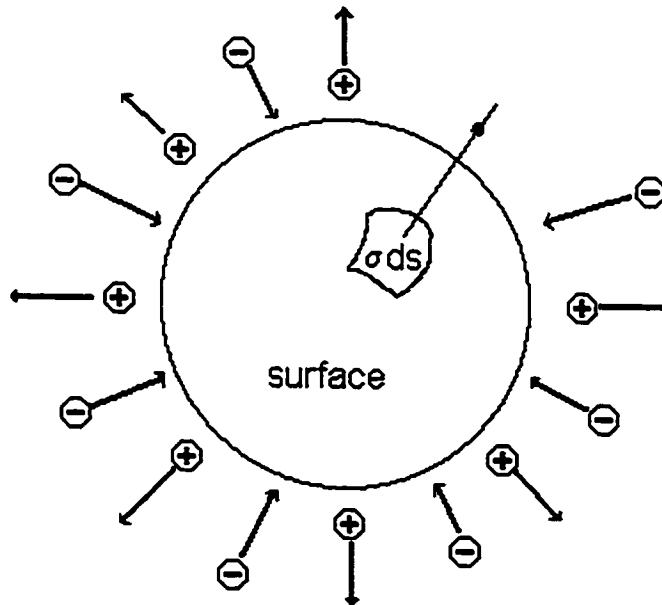


Figure 12. Charge decay through ionized air from a surface.

$$E = \frac{\sigma}{\epsilon_0} \quad (20)$$

$$j_{\text{ion}}^+ = Eeu^+n^+ \quad (21)$$

$$j_{\text{ion}}^- = Eeu^-n^- \quad (22)$$

$$\sigma^+ = \sigma_o^+ \exp\left(-\frac{t}{\epsilon_o\rho^-}\right), \quad (23)$$

In Equations 20-23, σ is the surface charge density, σ_o is the surface charge density, ϵ_o is the permittivity of air, e is the electron charge ($1.602 \times 10^{-19}C$), μ^- and μ^+ are the mobility of the negative and positive ions, and n^- and n^+ are the concentration of the positive and negative ions.

3.3 Case study of surface charge decay across the surface (run-off)

Surface charge decay across the surface involves the migration of surface charge across the surface. The migration of charges can be referred to as conduction of charges across the surface. Thus, surface charge decay is discussed here in terms of surface charge conductivity. On the subject of surface charge conductivity, Wintle (12) had report two kinds of surface charge conduction. One is the charge-driven surface charge conduction in which the electric field generated by the charges themselves is the source for conduction. Any other sources for conduction will contribute to what is referred to as natural conduction. Table 2 list relevant equations for the each type of surface charge conduction mentioned above.

The equations in Table 2 were applied to the Faraday cage experimental set-up and numerical solutions were attained and compared to experimental results of Liesegang et al.. Basically, the Faraday cage experiment involved putting a sample (charged sheet of insulator) into a cylindrical metal container that is connected to an electrometer. The outer surface of the container acquires the same charge as the sample. The capacitance of the cage to ground generates a voltage, which is then measured. Figure 13 shows the Faraday cage experiment set-up.

The numerical solutions pointed out that decay curves for charge-driven and natural-decay are similar during the beginning of the decay. In other words, it is hard to distinguish between charge-driven decay and natural-conduction decay during the initial decay time. However, when the decay is allowed to run for a longer time, then the curves

do separate. Wintle compare the numerical solutions with the Faraday cage experimental data for glass reported by Liesegang et al.. (9) The experimental data for glass tends to follow the natural-conduction decay process reasonably well.

Table 2. Summary of electrical properties related to surface charge conduction.

Surface conduction	Natural Conduction
Current Density	$j = cE = cE_{\max} A(x)T(t) = c \frac{\sigma_{\max}}{\epsilon_0} fA(x)T(t)$
Decay Function	$T(t) = \exp(-\alpha t / \tau)$
Characteristic time	$\tau = \frac{\epsilon_0 L}{cf}$
Charge-driven Conduction	
Current Density	$j = \mu cE = \mu cE_{\max} A(x)T(t) = \mu c \frac{\sigma_{\max}}{\epsilon_0} fA(x)T(t)$
Decay Function	$T(t) = \frac{1}{1 + \alpha t / \tau}$
Characteristic time	$\tau = \frac{\epsilon_0 L}{\sigma_{\max} \mu f}$

c = conductivity

$\epsilon_0 = 8.854 \times 10^{-12}$ F/m

E = electric field

E_{\max} = maximum electric field

$A(x)$ = dimensionless functions of position

f = dimensionless parameter that depends on the particular geometry ~ 1

L = length of the sample along the direction of charge motion

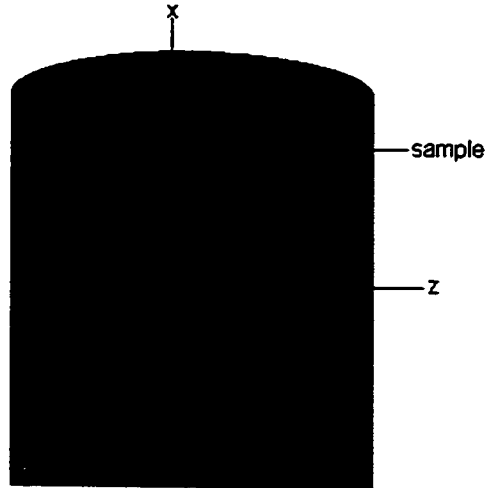


Figure 13. Simplified drawing of Faraday cage of cross-section, with a charged sheet sample hanging from the grounded clip at the top.

The experimental data reported by Liesegang et al. mentioned above was based on the study of a charge diffusion model for surface charge decay across the surface. Their two dimensional derivation resulted in a current density expression given by Equation 24. Equation 25 predicts the time dependent measure voltage.

$$j_x = \sigma_v E_x \quad (24)$$

$$1/V = \left(\frac{C}{\Delta z q 2A} \right) \left(\frac{q^2 D}{\epsilon \epsilon_0 kT} \right) + \frac{1}{V_0} \quad (25)$$

$$\sigma_v = n_v q^2 D / kT \text{ (ionic conductivity)} \quad (26)$$

E_x = electric field in the x direction

C = capacitance

C = capacitance

Δz = charged surface layer

A = surface area of the sample

$$n_v = \frac{1}{\left(\frac{q^2 D}{\epsilon \epsilon_0 k T}\right) t + \frac{1}{n_{v_0}}} \quad \text{(average concentration of the surface)} \quad (27)$$

$$n_{v_0} = V_0 C / q 2 A \quad \text{(initial surface ionic concentration)} \quad (28)$$

$$Q = 1.606 \times 10^{-19} \text{ C}$$

ϵ = permittivity of material under test

$$\epsilon_0 = \text{permittivity of space} = 8.854 \times 10^{-12} \text{ F/m}$$

$$k = \text{Boltzman constant} = 8.314 \times 10^{-23}$$

T = temperature

t = time

D = diffusion coefficient

The above model was tested on glass and the decay is shown in Figure 14. These plots reveal that the decay is not exponential. Figure 15 also shows the (1/V versus time) plot

the prediction of Equation (25). Plots such as that shown in Figure 15 provide initial surface conductivity (σ_{initial}), initial surface ionic concentration ($n_{s0} = V_0 C / q2A$), and initial surface resistivity (ρ_{initial}).

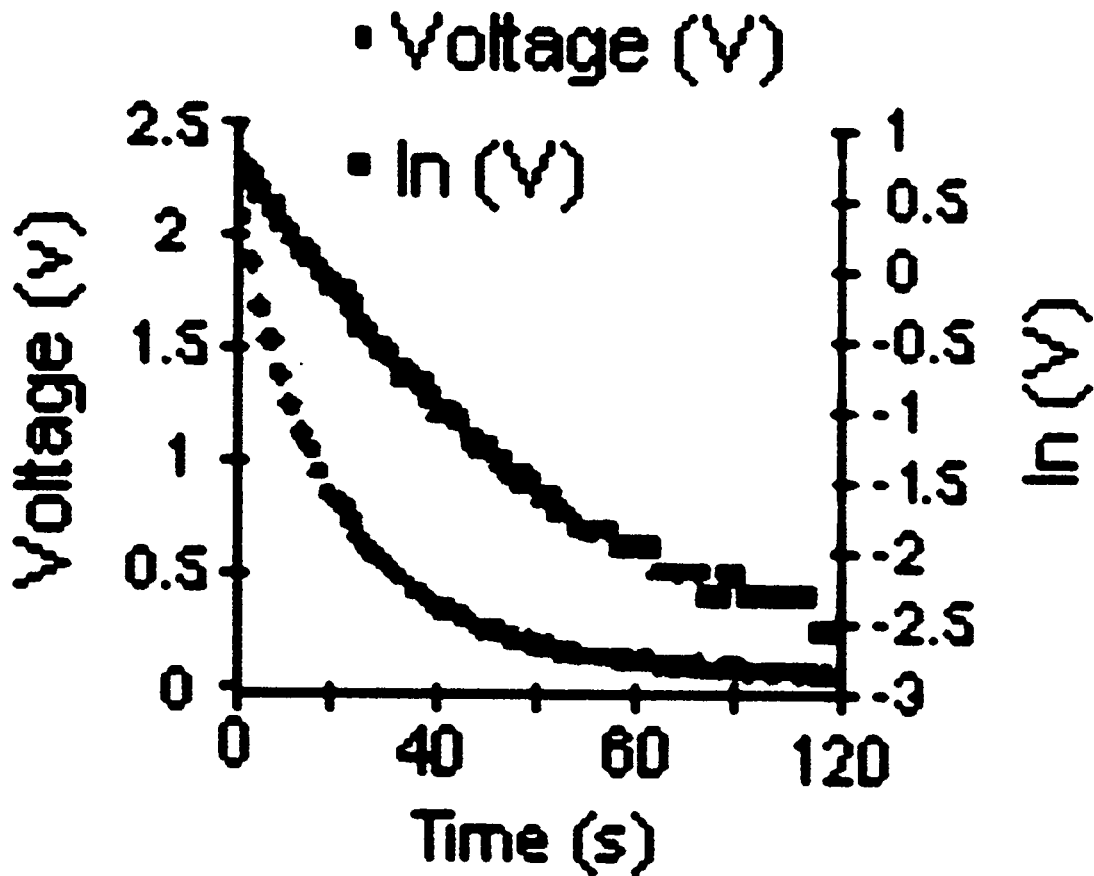


Figure 14. Charge decay plot for glass as measured in volt. From Lisegang et al. [9]. Reprinted with permission from the American Institute of Physics.

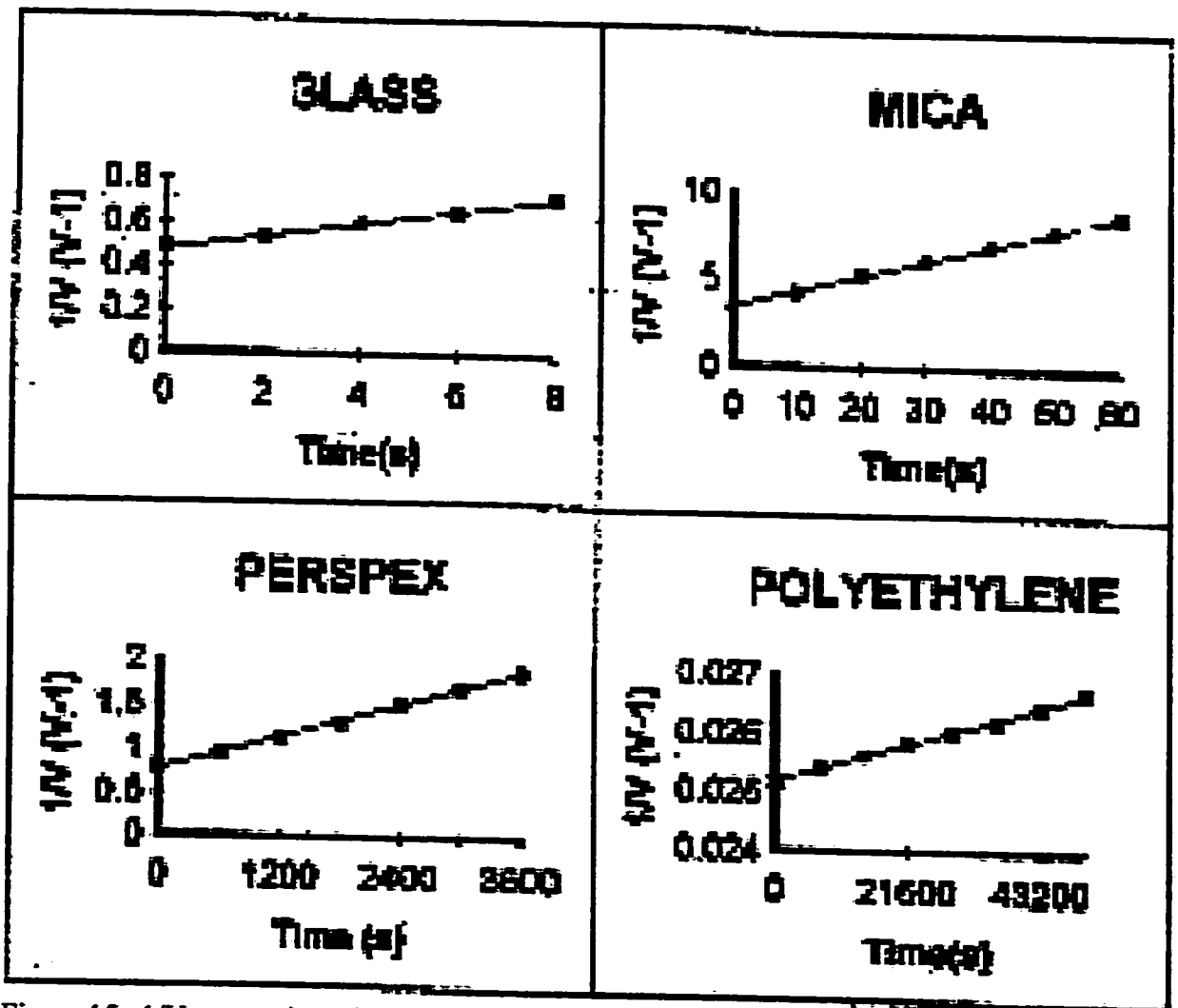


Figure 15. $1/V$ versus time plots for various materials. The plots allow the determination of initial values such as V_{initial} and σ_{initial} . From Lisevang et al. [9]. Reprinted with permission from the American Institute of Physics.

CHAPTER 4 – ELECTRIFICATION APPARATUS

4.1 Electrification Apparatus – System Components

In this chapter, the components of the electrification apparatus are presented. In section 4.2 the materials used in the experiment are reported. In addition, their characteristics prior to and after C.E. are discussed. Section 4.3 discusses the experimental procedures.

The electrification apparatus consists of a movable stage, which can be moved between the contact and the probe. The probe, which measures the surface potential, is connected to the Isoprobe Electrostatic Voltmeter 244. Figure 16 shows the essential components of the system with the necessary data acquisition instrument and software. It must be pointed out that the voltage readings of surface potential with the electrostatic voltmeter depends on the distance between the sample surface and the probe. Thus, it is necessary to make all measurements are at the same separation distance.

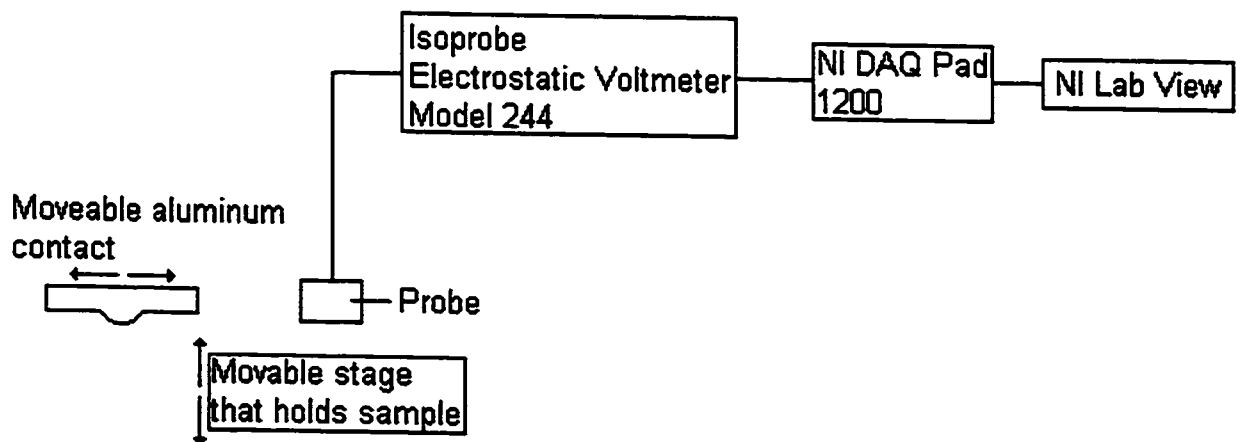


Figure 16. Basics components of electrification apparatus with data acquisition.

The Isoprobe Electrostatic Voltmeter measures the difference in voltage between the surface and the “circuit common.” In these experiments, a continuous monitoring or “voltage following” process is carried out, during which the difference in voltage between the surface and the “circuit common” decreases to zero. When the difference is zero, the circuit common will have attained the same potential as that of the surface under test. Thus, connecting the circuit common to ground will provide a reading of the potential of the sample surface under test.

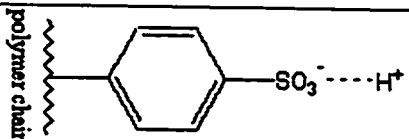
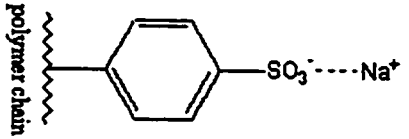
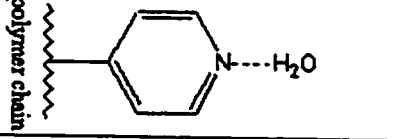
4.2 Electrification apparatus – Materials used to test apparatus

The key material characteristic of copolymers is the presence of an attached ionic group along the main polymer chain. The three copolymers considered in this experiment were sulfonated polystyrene-butylmethacrylate copolymer (SS-BUMA), sodium salt of sulfonated polystyrene-butylmethacrylate copolymer (SS-BUMA Na salt), and polystyrene-2-vinylpyridine copolymer (PS-2-VP). Their respective side-attachment groups are SO_3H^+ , SO_3Na^+ , and H_2O . In particular, the group SO_3^- is “anchored” to the main polymer chain and is not easily removed. On the other hand, the ions (H^+ and Na^+) are “loosely” associated to the SO_3^- group to provide charge neutrality, thus they (ions) are easily removed under C.E.. The H^+ and the Na^+ ions will therefore be referred to as “mobile” ions in contrast to the non-mobile ion SO_3^- group. As can be seen, such mobile ions are not found on the H_2O molecule – the whole H_2O is the mobile group which is neutral. However, it is possible for H_2O to split up into H^+ and HO^- with the prediction that HO^- will be the mobile ion. Table 3 summarizes the above mentioned materials characteristics.

As C.E. was performed, it was anticipated that the mobile ions would be transferred to the contacting materials, which were either metal or insulator. For example, with SS-BUMA which has the side-attached group SO_3H^+ , C.E. will have transferred the mobile ions H^+ from the sample surface to the contact material and leave behind an excess of the opposite polarity ions, which in this case is negative. Table 3 summarizes

the anticipated sample polarity as a result of transfer of mobile ions (and mobile neutral H₂O group) under C.E..

Table 3. Summary of material structure, their charge characteristics relevant to C.E..

Copolymers	Physical Characteristics	Structure	Side Group	Mobile ion	Polarity before C.E.	Anticipated polarity after C.E.
SS-BUMA	Powder		SO ₃ H ⁺	H ⁺	Positive	Negative
SS-BUMA Na salt	Powder		SO ₃ Na ⁺	Na ⁺	Positive	Negative
PS-2-VP	Chunk		H ₂ O	H ⁺ or HO ⁻	Neutral	Positive or Negative

4.3 Electrification apparatus – Test procedures

The experiment consisted of two stages. The first stage consisted of measurements to confirm the functionality of the electrification apparatus. This included confirming the apparatus' ability to distinguish between different materials, e.g. air, grounded metal surface and the three chosen materials mentioned above. In addition, measurements were taken to validate the repeatability of the apparatus.

The second stage of the experiment was to verify the phenomenon of C.E. (transfer of charges upon contact) for three materials mentioned above. The materials used for contact were metal (aluminum alloy) and insulator (vinyl). The contact consisted of a touch, swipe and rubbing. The time duration for these contacts was not monitored, i.e. some contacts were longer than others. The time duration of the contacts varied from sample to sample of the same materials as well as between materials to materials. In this experiment, an attempt was made to attain the maximum transferred-charge, which correlates to measured surface potential.

All the data were acquired using Labview and the National Instrument data acquisition instrument DAQ Pad1200. Mainly, the voltage readings were monitored and recorded as a function of time.

CHAPTER 5 – DATA ANALYSIS

5.1 Analysis for stage 1 – Validating instrument functionality and repeatability

In this chapter the analysis of the experimental results are discussed. Section 5.1 contains the discussion that is to confirm the functionality and repeatability of the electrification apparatus. Section reports and explains the observed oscillatory signal pattern. In Section 5.3 the contact electrification results are presented and discussed to confirm the predicted mobile ions. Section 5.4 reports and discusses the maximum potential attained under contact electrification. Last, Section 5.5 reports observed pressure effect.

Based on the measurements of air, the surface of the grounded metal and that of the three materials, it was concluded that the electrification apparatus was capable of generating distinctive voltage signals for the various materials. In particular, polarity differences are recorded for the different kind of copolymer material. Figures 17 shows plots of the voltages as a function of time for air and the grounded metal. Figures 18, 19 and 20 show plots of two-trial readings of surface potential of the materials PS-2-VP, SS-BUMA and SS-BUMA Na salt respectively. Figures 17, 18, 19, 20 show that the surface potential is different in magnitude as well as in polarity. Comparing these surface potential curves with that of air, it can be seen that stabilization of surface potential was slower for air. The difference between the two trials for air seen during the initial measure is in fact misleading. After data for Trial 1 was taken, the electrostatic voltmeter was turned off for about 5 seconds. Then the electrostatic voltmeter was turned back on for Trial 2 measurements. It is believed that the electrostatic voltmeter was still retaining

insufficient to allow the electrostatic voltmeter to really erase any “memory” of the previous measurement. In other words, the initial data of Trial 2 is actually the final data of Trial 1. Overall, the trials show repeatable results for all tested materials.

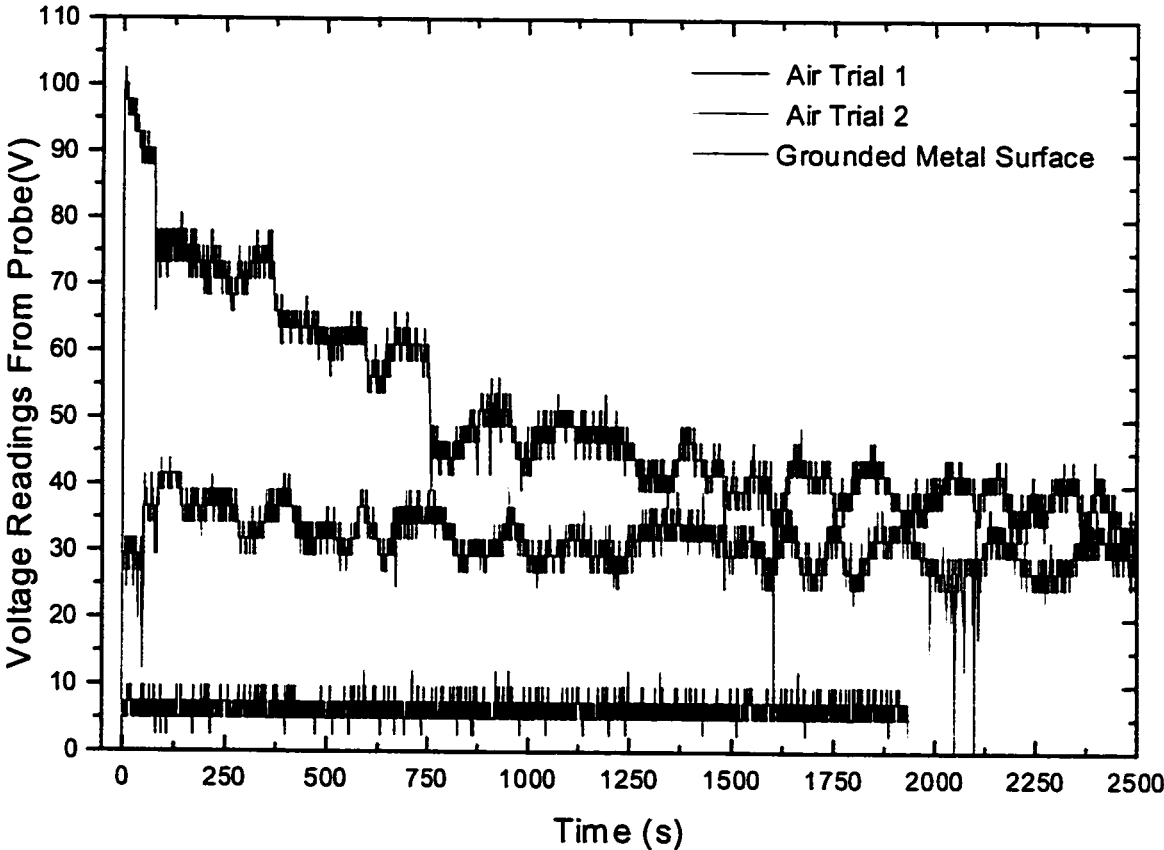


Figure17. Voltage readings of air and grounded metal surface.

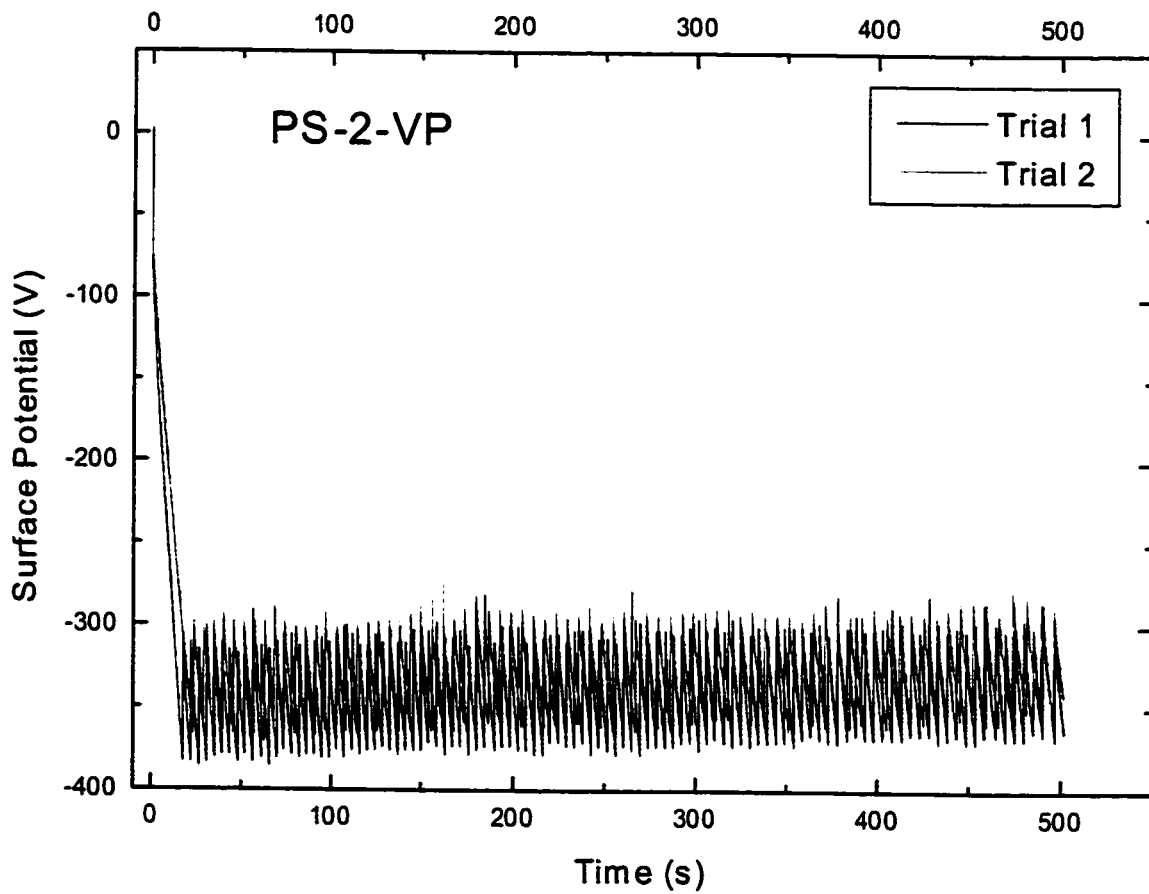


Figure 18. Repeatability of surface potential measurements of PS-2-VP.

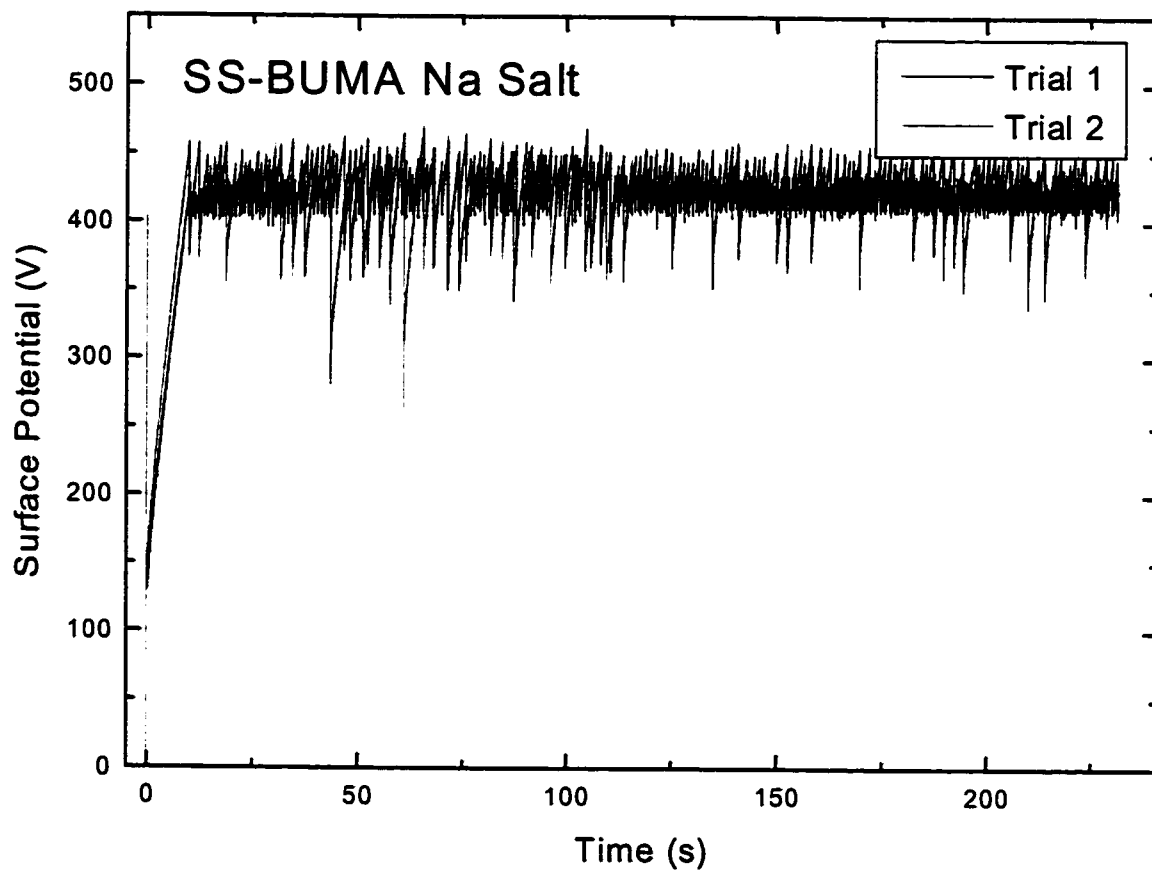


Figure 19. Repeatability of surface potential measurements of SS-BUMA Na salt.

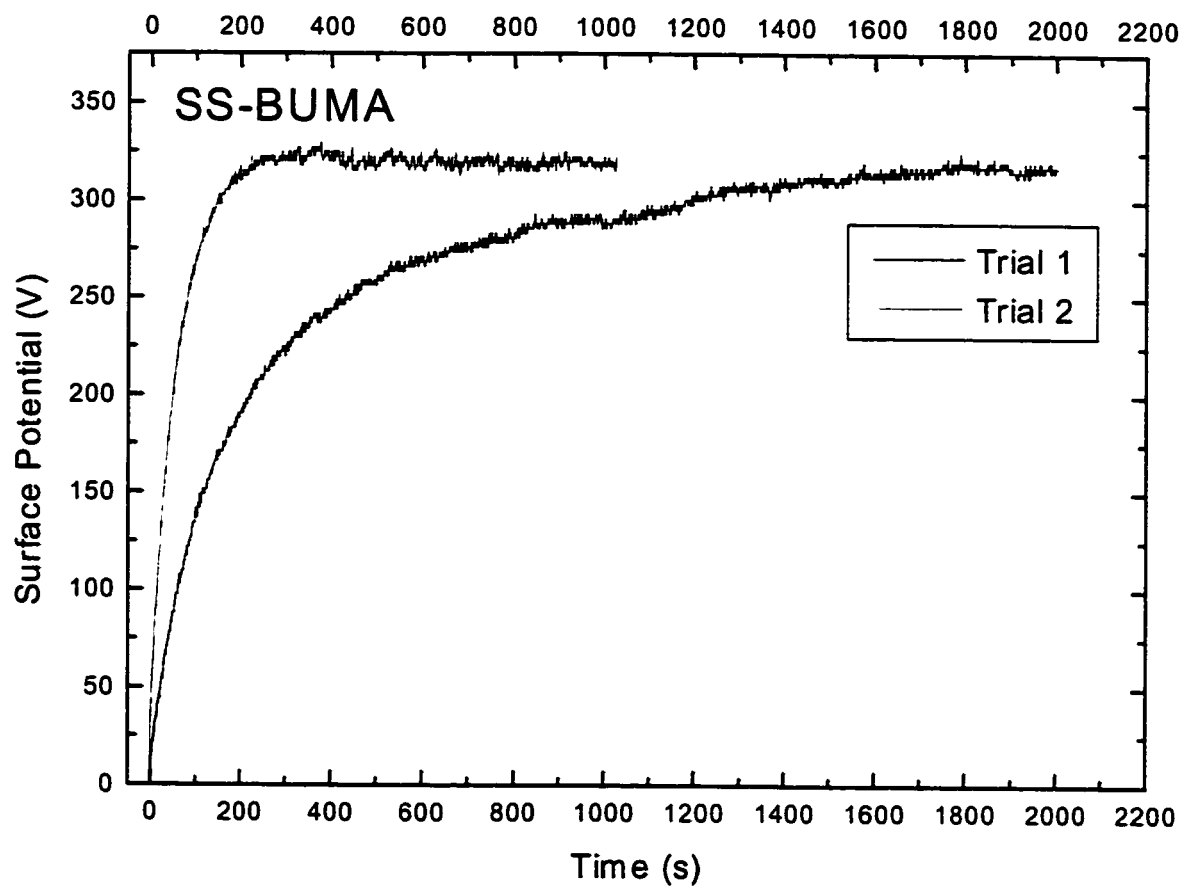


Figure 20. Repeatability of surface potential measurements of SS-BUMA.

5.2 Analysis for stage 1 – Oscillatory signal Pattern

In the measurements to validate the functionality of the Isoprobe Electrostatic Voltmeter, an oscillatory signal-pattern was observed. Figure 21 shows the oscillatory pattern of surface potential for PS-2-VP with a period of 4.5s and voltage range of 64V. As can be seen it is very regular. Voltage readings for SS-BUMA Na salt show this oscillatory signal pattern as shown in Figure 22. The oscillatory signal pattern for SS-BUMA Na salt is somewhat different from that of PS-2-VP. There is a minor period and a random major oscillations as can be seen in Figure 22. The minor period is between point 2 and 3, and 3 and 4 as shown in Figure 22 with 1s period time and voltage range of 44V. The major random oscillations such as locations 1 and 4, and 4 and 5 are believed to be random charge fluctuations. This indicates that SS-BUMA Na salt surface charges are easily disturbed compared with PS-2-VP. Figure 23 reveals that SS-BUMA has an unclear oscillatory signal pattern, indicating surface charges for this material are relatively stable. Points such as 1, 2, 3 seem to indicate oscillatory signal pattern. Thus, an observational analysis, one can qualitatively determine the degree of surface charge stability in terms of charge fluctuation for these materials.

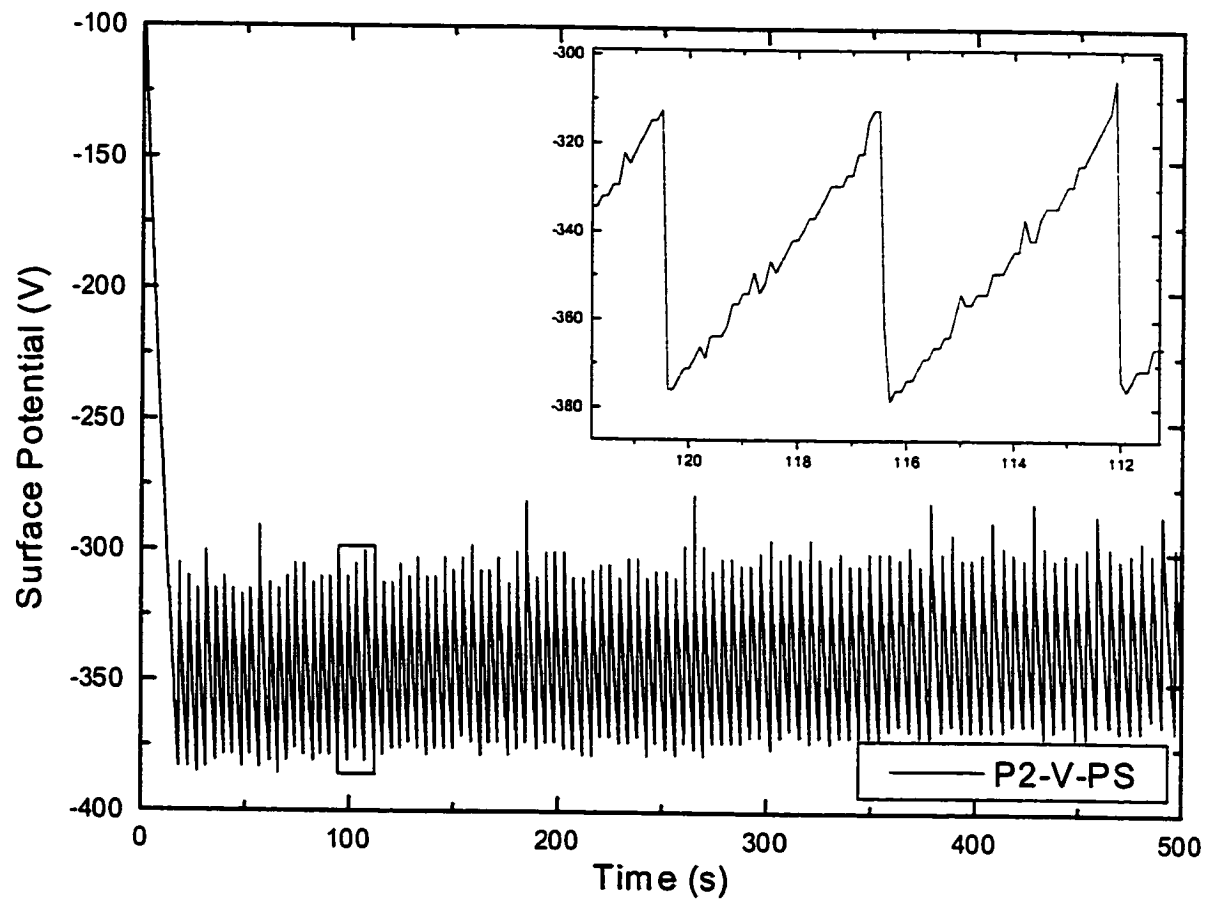


Figure 21. Surface potential of PS-2-VP pellet-form sample as a function of time.

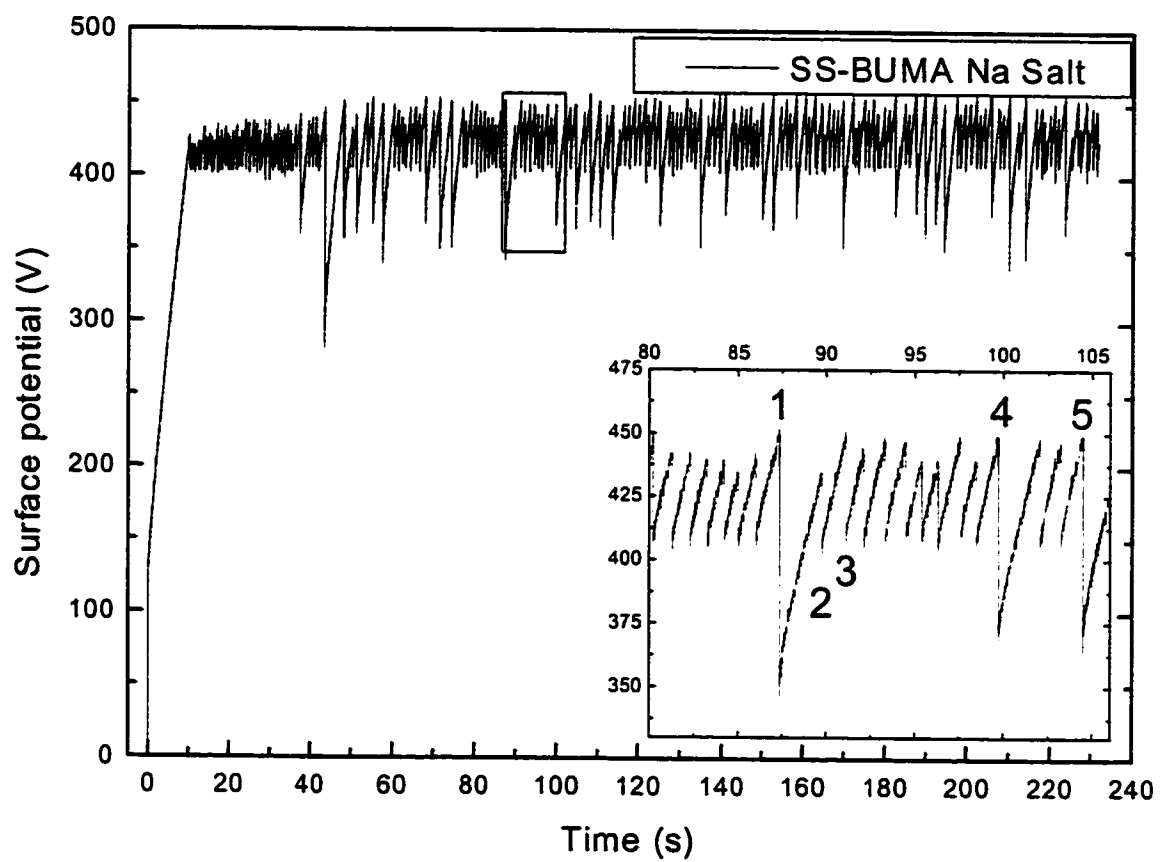


Figure 22. Surface potential of SS-BUMA-Na Salt pellet-form sample as a function of time.

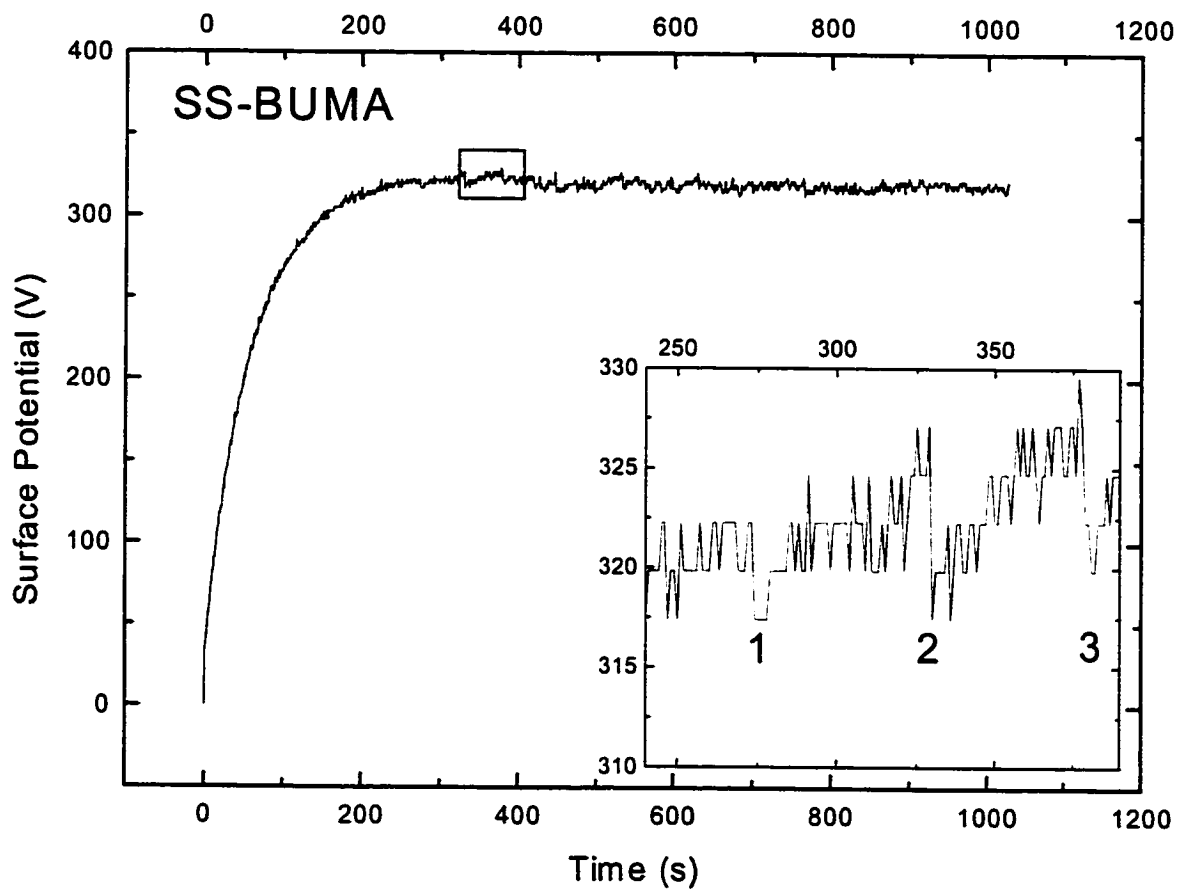


Figure 23. Surface potential of SS-BUMA pellet-form sample as a function of time.

5.3 Analysis for stage 2 – Confirming C.E. with potential polarity

For SS-BUMA, a metal contact was used and the contact was in the form of touch and swipe. C.E. performed for SS-BUMA, which is in raw form, reveals a change in polarity of the potential from positive to negative as predicted. Figure 24 shows the evolution of the potential and the contact sequence.

With the other two materials, SS-BUMA Na salt and PS-2-VP, the C.E. study was somewhat involved and is explained as follow. Because SS-BUMA Na salt and PS-2-VP were powders, a specimen with a flat surface had to be created. The flat surface condition was achieved by making pellets from the powder. Schematic of the pellet-making process is illustrated in Figure 25. As can be seen, this pellet-making process exposed the materials to C.E. - one surface of the pellet was contacted with metal and the other surface with an insulating material (weight paper). Because of C.E., the charge's polarity of the pellets may disagree with the sign predicted in Table 3, which lists the potential polarity before the pellets were made, i.e. prior to any kinds of contact. The polarity information after the pellets were made is listed in Table 4. The polarity information before and after pellet formation, indicates that a metal contact caused minimal charge transfer of the SS-BUMA Na salt. Conversely, the weight paper (insulator) did charge the pellet during the pellet-making process. In the case of PS-2-VP, contact charging occurred with both metals and insulators. There was not enough evidence to determine whether insulator or metal is more effective in contact charging of PS-2-VP.

In terms of the theory that charge results from the transfer of ions, the attached H₂O in PS-2VP is neutral, and expected to impose zero potential. However, the H₂O dissociate into H⁺ and OH⁻. Thus under C.E. either H⁺ or OH⁻, or both ions can be transferred. The positive surface charge produced by C.E. on the pellet (Table 5) suggests that the H₂O molecule dissociates and net negative charges are removed from the sample surface. This suggests that OH⁻ is more mobile than H⁺.

Table 4. Surface potential polarity as a result of pellet formation

Material	Polarity under different contact material	
	Metal	Insulator (weight paper)
PS-2-VP	Positive (680V)	Positive (680)
SS-BUMA Na salt	Positive (1221V)	Negative (-1204V)

5.4 Analysis for stage 2 – Measuring maximum potential under C.E.

The maximum potential for the three materials attained under electrification are listed in Table 5. Listed also are the contact materials used for C.E. As can be seen, reproducible maximum potentials were observed. The polarity as a result C.E. was negative as expected for SS-BUMA and SS-BUMA Na salt. The delta in potential for SS-BUMA and SS-BUMA Na salt, which corresponds to the amount of charge transferred, is $\sim -1500V$. The charge density associated with these potentials was calculated using an approximated probe sampling area. The surface sampling area is approximated by using the area of the probe opening $\sim 2.54 \times 10^{-6} \text{ m}^2$ (diameter of the probe is 1.8mm). With the above contact area, the surface potential is $\left(\frac{1500V}{2.54 \times 10^{-6} \text{ m}^2} \right)$ or $\sim 590 \times 10^6 \text{ V/m}^2$.

5.5 Analysis for Stage 2 – Pressure effect

A pressure dependence on the charge transfer was observed with SS-BUMA Na salt. During the preparation of the SS-BUMA-Na salt, a potential of -1204V was produced on weight-paper-contact side of the pellet and 1221V on the metal-contact side. The metal-pressed side of the pellet was chosen to carry out the C.E. with an insulator (vinyl) as contact material. During C.E. the polarity change (positive to negative) was confirmed. The maximum magnitude of the measured potential from C.E. (touch, rub, and swipe) is ~ -350V. However, the maximum should at least be -1204V as found during the making of the pellet. The high value -1204V may result from the high applied pressure (1500psi) used to press the pellet. Since the applied C.E. (touch, rub, and swipe) had minimal applied pressure, the resulting maximum potential was only -350V.

Finally, it is important to comment on the observed oscillatory behavior in the raw data. The effect may be linked to the function of the electrostatic voltmeter, since the instrument operates with an imbedded oscillatory signal source.

Table 5. Surface potential prior to and after C.E. with the associated contacting material

Material	Contact materials	Initial surface potential prior to C.E		Maximum surface potential attained under C.E.		Delta in surface potential under C.E.	
		Sample 1	Sample 2	Sample 1	Sample 2	Sample 1	Sample 2
PS-2-VP	Insulator	680V	680V	~ 988V	~ 1088V	308V	408V
SS-BUMA Na salt	Insulator	1221V	1240V	~-360V	~-352V	-1581V	-1592V
SS-BUMA	Metal	846V	676V	~-539V	~-969V	-1385V	-1645V

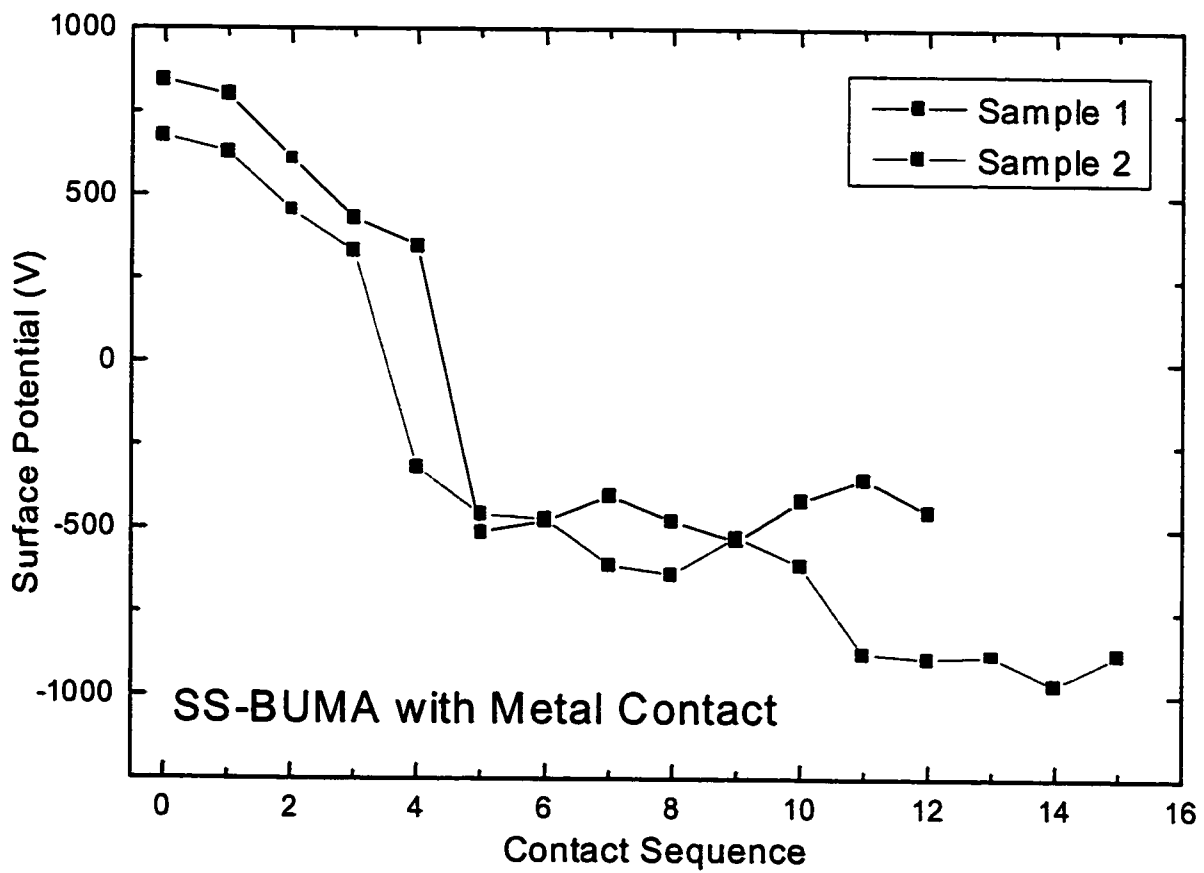


Figure 24. Evolution of surface potential versus number of contact for SS-BUMA.

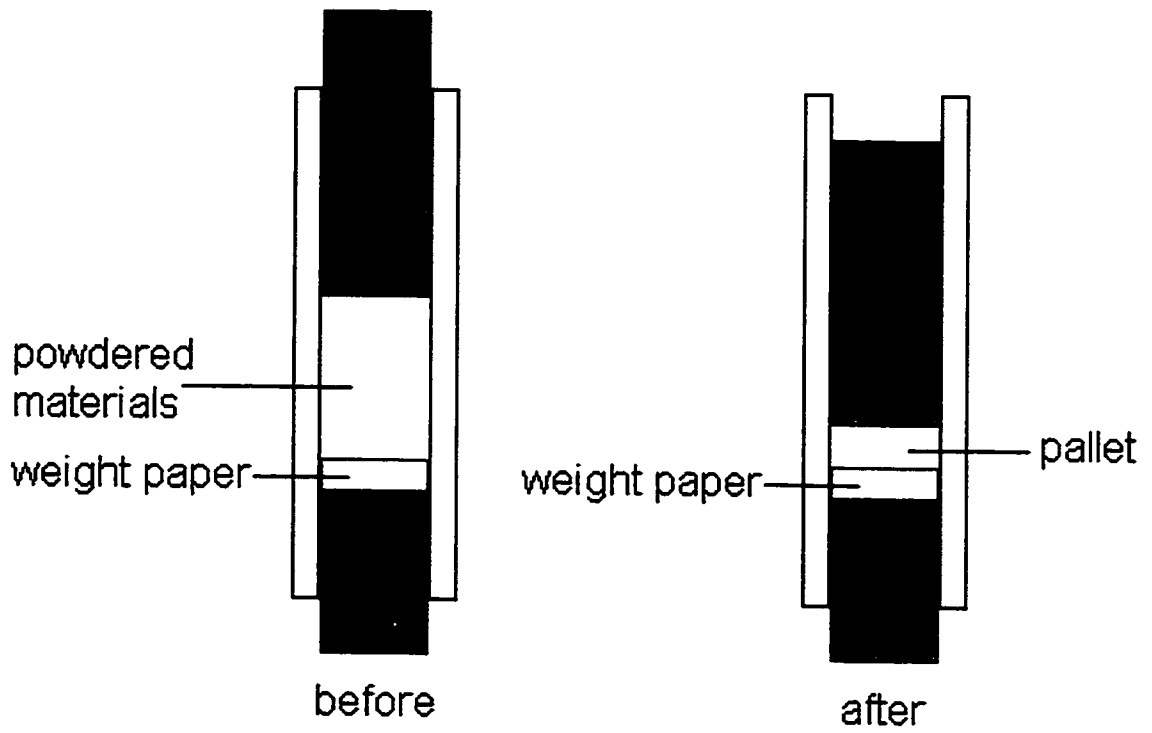


Figure 25. Schematic of pellet making device and process.

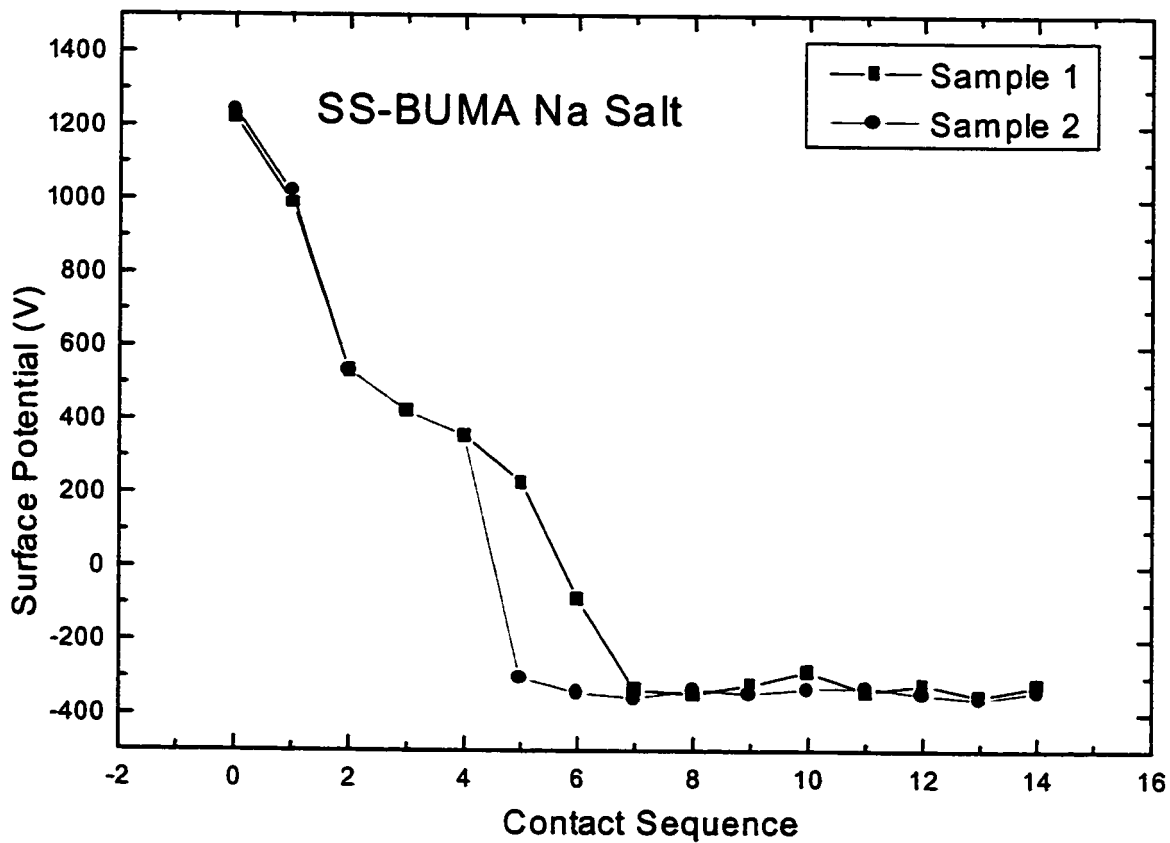


Figure 26. Evolution of surface potential versus number of contact for SS-BUMA Na salt.

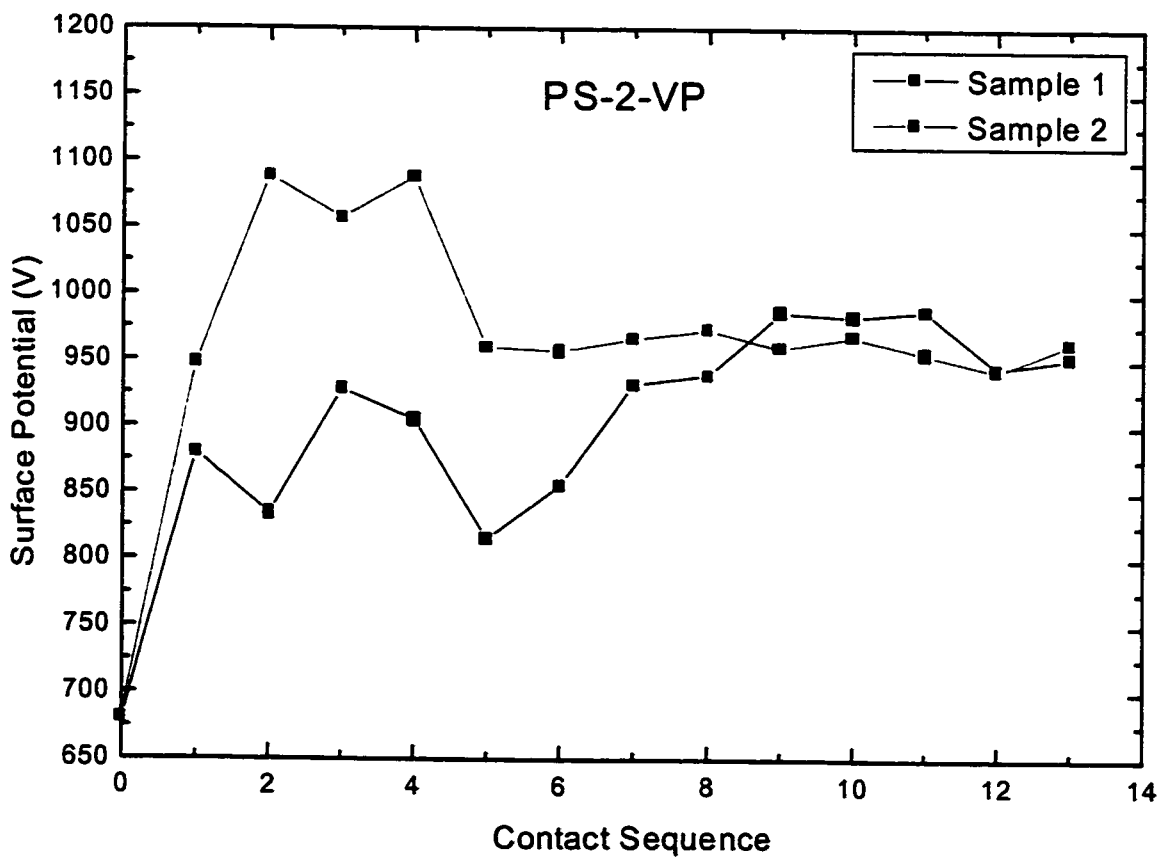


Figure 27. Evolution of surface potential versus number of contact for PS-2-VP.

CONCLUSION

The results of the measured polarity before and after extended contacts are consistent with the existence of mobile ions and the transfer of these ions due to C.E. for SS-BUMA and SS-BUMA Na salt. Table 3 lists the mobile ions for SS-BUMA and SS-BUMA Na salt. Data for PS-2-VP implies that the OH^- is the mobile ion. The experiment was successful in attaining the maximum potential values for all materials and to show distinctive characteristics, i.e. different polarity and magnitude. Thus, the electrification apparatus was confirmed to be valuable for carrying out in-depth C.E. research. In addition, this thesis also contains procedures to operate the electrification apparatus.

APPENDIX I – Derivation of Equation 2

The derivation presented here is provided by Wangness (10). The electric given by Equation 2 is specific for the case of a uniform infinite plane sheet of surface charge. We want to know what I the electric at a point P due to a uniform infinite plane sheet of surface charge. We start with the general Equation 1 as our first step. In this derivation, the bold type indicates a vector quantity.

$$\text{Step 1: } \mathbf{E}(\mathbf{r}) = \frac{1}{4\pi\epsilon_0} \int_S \frac{\sigma(\mathbf{r}')\hat{R}d\mathbf{a}'}{R^2}$$

\hat{R} = radial unit vector

ϵ_0 = permittivity of free space = 8.854×10^{-12} F/m

Figure 28 shows the system configuration for this derivation.

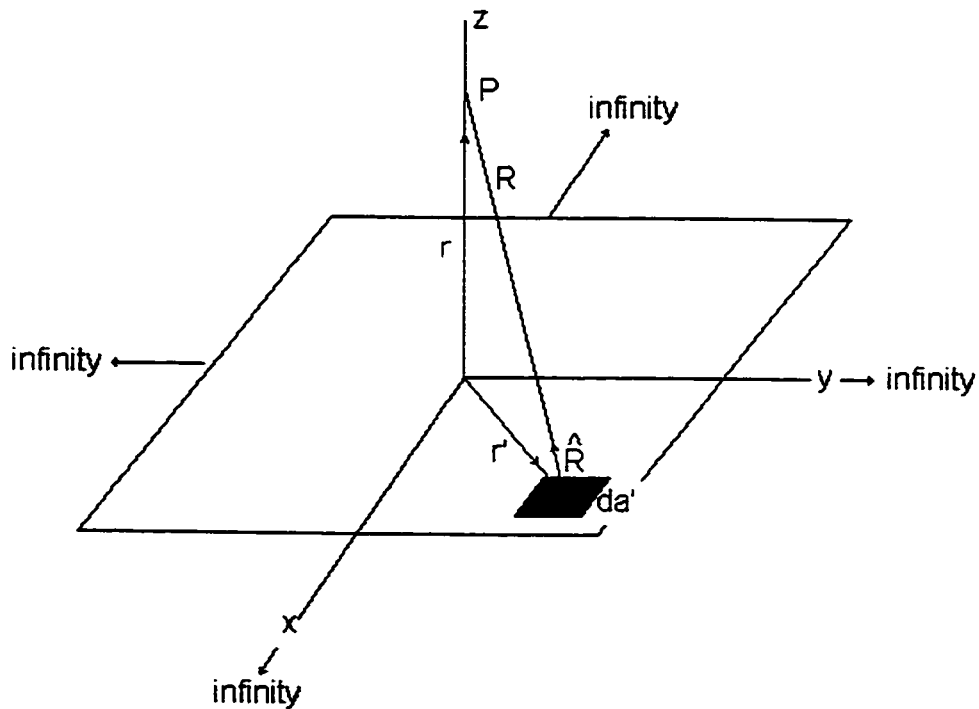


Figure 28. Diagram schematic of the field due to a uniform infinite plane sheet.

Figure 28. Diagram schematic of the field due to a uniform infinite plane sheet.

Since the surface charge density is constant for this case, we can replace $\sigma(r')$ with σ in

Step 1.

$$\text{Step 2: } \mathbf{E}(\mathbf{r}) = \frac{1}{4\pi\epsilon_0} \int_S \frac{\sigma \hat{\mathbf{R}} da'}{R^2}$$

Now express R^2 and $\hat{\mathbf{R}}$ in rectangular coordinates.

$$\mathbf{R} = \mathbf{r} - \mathbf{r}' = (x - x')\hat{\mathbf{x}} + (y - y')\hat{\mathbf{y}} + (z - z')\hat{\mathbf{z}}$$

$$R = \left[(x - x')^2 + (y - y')^2 + (z - z')^2 \right]^{1/2}$$

$$R^2 = (x - x')^2 + (y - y')^2 + (z - z')^2$$

$$\hat{\mathbf{R}} = \frac{\mathbf{R}}{R} = \frac{(x - x')\hat{\mathbf{x}} + (y - y')\hat{\mathbf{y}} + (z - z')\hat{\mathbf{z}}}{\left[(x - x')^2 + (y - y')^2 + (z - z')^2 \right]^{1/2}}$$

Now substitute into Step 2.

$$\text{Step 3: } \mathbf{E}(\mathbf{r}) = \frac{1}{4\pi\epsilon_0} \int_S \frac{\sigma \frac{(x - x')\hat{\mathbf{x}} + (y - y')\hat{\mathbf{y}} + (z - z')\hat{\mathbf{z}}}{\left[(x - x')^2 + (y - y')^2 + (z - z')^2 \right]^{1/2}}}{(x - x')^2 + (y - y')^2 + (z - z')^2} da'$$

Now replace da' with $dx' dy'$ and combining terms.

$$\text{Step 4: } \mathbf{E}(\mathbf{r}) = \frac{\sigma}{4\pi\epsilon_0} \int_S \frac{(x - x')\hat{\mathbf{x}} + (y - y')\hat{\mathbf{y}} + (z - z')\hat{\mathbf{z}}}{\left[(x - x')^2 + (y - y')^2 + (z - z')^2 \right]^{3/2}} dx' dy'$$

Now expanding the surface integral from $-\infty$ to ∞ in the x and y directions.

$$\text{Step 5: } \mathbf{E}(\mathbf{r}) = \frac{\sigma}{4\pi\epsilon_0} \int_{-\infty}^{\infty} \int_{-\infty}^{\infty} \frac{(x - x')\hat{\mathbf{x}} + (y - y')\hat{\mathbf{y}} + (z - z')\hat{\mathbf{z}}}{\left[(x - x')^2 + (y - y')^2 + (z - z')^2 \right]^{3/2}} dx' dy'$$

Because we have chosen the point P to lie on the z-axis $x' = y' = 0$. Furthermore, the plane sheet of at the origin, $z' = 0$. With that we rewrite Step 5.

$$\text{Step 6: } \mathbf{E}(\mathbf{r}) = \frac{\sigma}{4\pi\epsilon_0} \int_{-\infty}^{\infty} \int_{-\infty}^{\infty} \frac{-x'\hat{\mathbf{x}} - y'\hat{\mathbf{y}} + z'\hat{\mathbf{z}}}{(x'^2 + y'^2 + z'^2)^{3/2}} dx' dy'$$

Now expanding the integral into x, y, z components of \mathbf{E} .

$$\mathbf{E}(\mathbf{r}) = \frac{\sigma}{4\pi\epsilon_0} \int_{-\infty}^{\infty} \int_{-\infty}^{\infty} \frac{-x'\hat{\mathbf{x}} dx' dy'}{(x'^2 + y'^2 + z'^2)^{3/2}} + \frac{\sigma}{4\pi\epsilon_0} \int_{-\infty}^{\infty} \int_{-\infty}^{\infty} \frac{-y'\hat{\mathbf{y}} dx' dy'}{(x'^2 + y'^2 + z'^2)^{3/2}} + \frac{\sigma}{4\pi\epsilon_0} \int_{-\infty}^{\infty} \int_{-\infty}^{\infty} \frac{z'\hat{\mathbf{z}} dx' dy'}{(x'^2 + y'^2 + z'^2)^{3/2}}$$

Step 7:

E_x

E_y

E_z

Since $\hat{\mathbf{x}}$ and $\hat{\mathbf{y}}$ terms in the integrand are odd functions of x' and y' , $E_x = E_y = 0$, and we can reduce Step 8.

$$\text{Step 8: } \mathbf{E}(\mathbf{r}) = \frac{\sigma \hat{\mathbf{z}}}{4\pi\epsilon_0} \int_{-\infty}^{\infty} \int_{-\infty}^{\infty} \frac{z dx' dy'}{(x'^2 + y'^2 + z'^2)^{3/2}} = \frac{\sigma \hat{\mathbf{z}}}{4\pi\epsilon_0} \int_{-\infty}^{\infty} z dx' \int_{-\infty}^{\infty} \frac{dy'}{(x'^2 + y'^2 + z'^2)^{3/2}}$$

Now integrating with respect to dy' .

$$\text{Step 9: } \mathbf{E}(\mathbf{r}) = \frac{\sigma \hat{\mathbf{z}}}{2\pi\epsilon_0} \int_{-\infty}^{\infty} \frac{z dx'}{(x'^2 + z'^2)}$$

Now integrating with respect to dx' .

$$\text{Step 10: } \mathbf{E}(\mathbf{r}) = \frac{\sigma \hat{\mathbf{z}}}{2\epsilon_0} \text{ (Equation 2 as reported in the discussion)}$$

APPENDIX II- ELECTRIFICATION APPARATUS OPERATING MANUAL

APPARATUS

1. Aluminum encasing
2. Handle – pull out to remove contact assembly
3. Screw cap – to release contact
4. Contact
5. Probe 1 - for measuring potential of sample surface
6. Stage - that holds sample
7. Probe 2 - for measuring potential of contact
8. Micrometer – Turn bottom knob to move Probe 2
9. Connections to control step motors – step motors are used to move stage and contact assembly

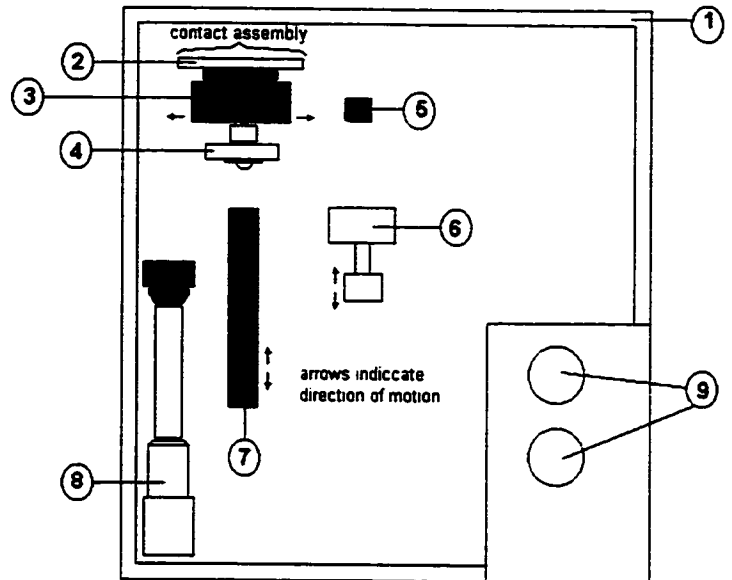


Figure 29. Schematic of electrification apparatus

MANUAL CONTROL OF STEP MOTORS

Two Stepper Driver, which are connected to the two step motors inside the apparatus, provide control motion of the contact assembly and Probe 1.

One Stepper Driver is used to control the horizontal motion of the contact assembly. The other is used to control the vertical motion of the stage.

The use of the Stepper Drive for electrification purposes consists of two basic features:

- Speed control – this controls the speed of the motion
- Direction control – this controls the direction of the motion (e.g. left, right, up and down).
 - The switches that control the direction are shown in Figure 2.
 - The silver switches are for continuous and jog motion. Switch upward for continuous motion. Switch downward and release for jog motion.

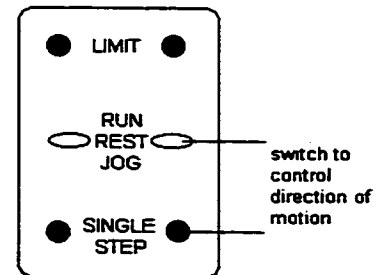


Figure 30. Direction-switch layout.

- The black switches are for a singles step motion (very small increment).
- Left switch for left (or up). Right switch for right (or down).

AUTOMATIC CONTROL OF STEP MOTORS

Automation of the step motors requires interfacing the SK1 Stepper Driver with a computer. This can be done with Labview and the DAQ Pad 1200. Basically, one sends digital signals to the serial port at the back of the SK1 Stepper Driver. Using Labview one sends digital signals to the DAD Pad 1200, which then pass those signals on to the SK1 Stepper Driver which drives the step motor one single step (0.005mm). The connection from the DAQ Pad 1200 to the SK1 Stepper Driver is shown in Figure 31.

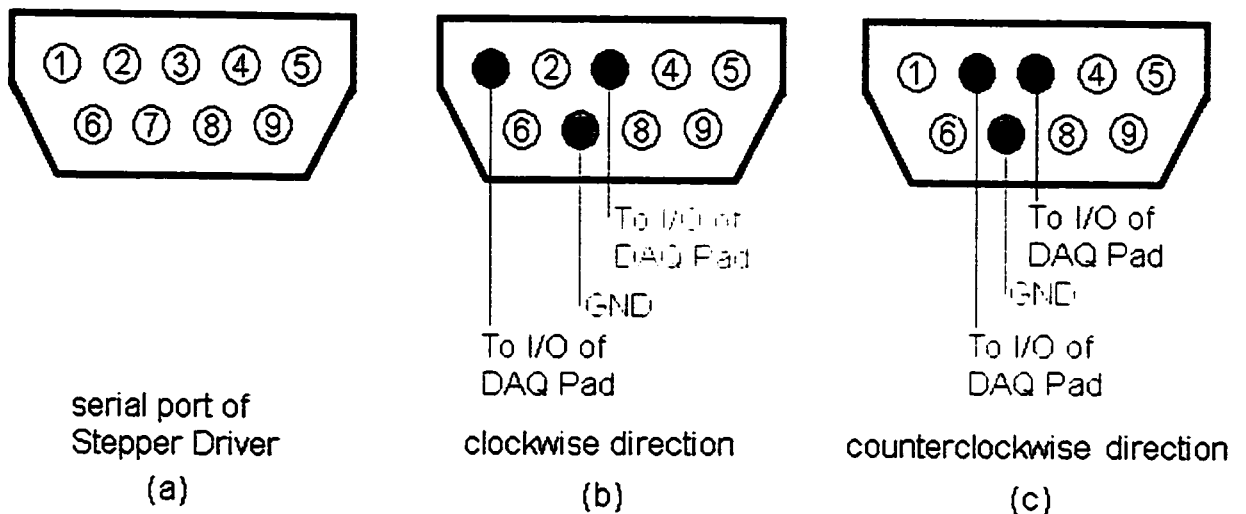


Figure 31. Pin connection configuration for controlling SK1 Stepper Driver.

MEASURE INSTRUMENTS

Two Isoprobe Electrostatic Voltmeters, model 244, which are connected to the two probes, provide readings of the surface potential in volt.

The probe sees the sample surface through a small hole on the probe (0.070" = 1.8mm

The probe sees the sample surface through a small hole on the probe (0.070" = 1.8mm dia). Thus the surface area being measured is about the same as that of the are of the hole. At a spacing of 0.005" (0.13mm) between sample surface and probe, the surface area under test is approximately 0.1" (2.54mm) in diameter.

Voltage signals from measurement of polymeric materials tend to fluctuate, thus it is recommended to record the data as a function of time and then take the average. Again use Labview and the DAQ Pad 1200 to acquire and save the data into a spread sheet format. Figure 32 show the connection necessary for the data acquisition process. Labview has several sample programs that can be use for the data acquisition.

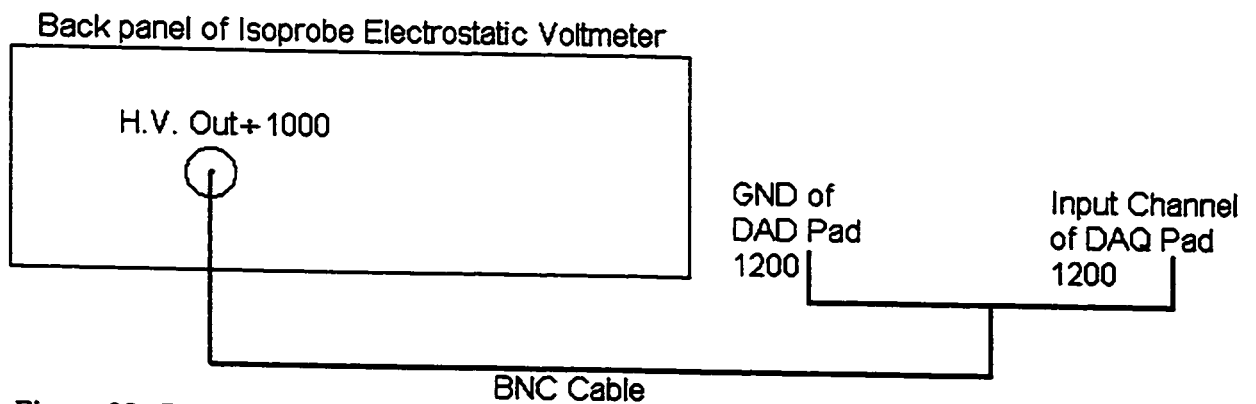


Figure 32. Connection form Isoprobe Electrostatic Voltmeter to DAQ Pad 1200 for data acquisition.

Reference

1. Baum, E.A., Lewis, T.J, Toomer, R. "The Decay of Surface Charge on n-octadecane Crystal." *Journal of Physics D: Applied Physics*, vol 11, 1978: 703-715.
2. Coelho, Roland, Levy Leon, Sarrail, Daniel. "On the Natural Decay of Corona Charged Insulating Sheets." *IEEE Trans. E.I.*, vol 22, 1986: 289-298.
3. Coelho, Roland, Levy, Leon, Sarrail, Daniel. "Charge Decay Measurements and Injection in insulators." *Journal of Physics D: Applied Physics*, vol 22, no. 9, 1989: 1406-1409.
4. Crowley, Joseph M.. Fundamentals of Applied Electrostatics. New York: John Wiley & Sons, 1986.5
5. Diaz, A. F.. "C.E. of Materials: The chemistry of Ions on Polymer Surfaces." *Journal of Adhesion*, Vol. 67, 1998: 111-122.
6. Harper, W.R.. Contact and Frictional Electrification. London: Oxford University Press, 1967.
7. Ieda, M., Sawa, G. and Shinohara U. "Decay of Electric Charges on Polymeric Films." *Electrical Engineering in Japan*, vol. 88, no. 6, 1968: 67-73.
8. Jonassen, Niels. Electrostatics. New York: International Thomson Publishing, 1998. Macur, Jiri and Karel Domansky. "Charge Injection into Insulators and Partial Discharge." *Japanese Journal of Applied Physics*, vol. 32, No. 11A, 1993: 5136-5137.
9. Liesegang, B. C. Senn, and E. R. Smith. "Resistivity of Static and Antistatic Insulators from Surface Charge Measurement." *Journal of Applied Physics*, vol. 77, 1995: 5782 – 5785.
10. Wangness, Roald K.. Electromagnetic Fields. New York: John Wiley & Sons, 1976.
11. Williams, Edgar M.. The Physics and Technology of Xerographics Processe. New York: John Wiley & Sons, 1984.
12. Wintle, H.J.. "Surface-Charge Decay in Insulators with Nonconstant Mobility and with Deep Trapping." *Journal of Applied Physics*, vol. 43, no. 7, 1972: 2927-2930.
13. Wintle, H.J. "Surface Condition on Insulators: Analysis and Interpretation of the Faraday Cage Experiment." *Journal of Applied Physics*, vol. 81, no. 6, Mar. 1997: 2682 – 2685.